Published in final edited form as:
Neuroimage. 2009 June ; 46(2): 432–446. doi:10.1016/j.neuroimage.2009.02.009.

T_1 weighted Brain Images at 7 Tesla Unbiased for Proton Density, T_2* contrast and RF Coil Receive B1 Sensitivity with Simultaneous Vessel Visualization

Pierre-François Van de Moortele[1], **Edwards J. Auerbach**[1], **Cheryl Olman**[1], **Essa Yacoub**[1], **Kâmil Uğurbil**[1], and **Steen Moeller**[1]

[1]Center for Magnetic Resonance Research (CMRR), Department of Radiology, University of Minnesota Medical School, Minneapolis, MN 55455, USA

Abstract

At high magnetic field, MR images exhibit large, undesirable signal intensity variations commonly referred to as “intensity field bias”. Such inhomogeneities mostly originate from heterogeneous RF coil B_1 profiles and, with no appropriate correction, are further pronounced when utilizing rooted sum of square reconstruction with receive coil arrays. These artifacts can significantly alter whole brain high resolution T_1-weighted (T_1w) images that are extensively utilized for clinical diagnosis, for gray/white matter segmentation as well as for coregistration with functional time series. In T_1 weighted 3D-MPRAGE sequences, it is possible to preserve a bulk amount of T_1 contrast through space by using adiabatic inversion RF pulses that are insensitive to transmit B_1 variations above a minimum threshold. However, large intensity variations persist in the images, which are significantly more difficult to address at very high field where RF coil B_1 profiles become more heterogeneous. Another characteristic of T_1w MPRAGE sequences is their intrinsic sensitivity to Proton Density and T_2* contrast, which cannot be removed with post-processing algorithms utilized to correct for receive coil sensitivity.

In this paper, we demonstrate a simple technique capable of producing normalized, high resolution T_1w 3D-MPRAGE images that are devoid of receive coil sensitivity, Proton Density and T_2* contrast. These images, which are suitable for routinely obtaining whole brain tissue segmentation at 7 Tesla, provide higher T_1 contrast specificity than standard MPRAGE acquisitions. Our results show that removing the Proton Density component can help identifying small brain structures and that T_2* induced artifacts can be removed from the images. The resulting unbiased T_1w images can also be used to generate Maximum Intensity Projection angiograms, without additional data acquisition, that are inherently registered with T_1w structural images. In addition, we introduce a simple technique to reduce residual signal intensity variations induced by Transmit B1 heterogeneity.

Because this approach requires two 3D images, one divided with the other, head motion could create serious problems, especially at high spatial resolution. To alleviate such inter-scan motion problems, we developed a new sequence where the two contrast acquisitions are interleaved within a single scan. This interleaved approach however comes with greater risk of *intra-scan* motion issues because of a longer single scan time. Users can choose between these two trade offs depending on specific protocols and patient populations.

Address for Correspondence: Pierre-Francois Van de Moortele, Center for Magnetic Resonance Research, 2021 Sixth Street S.E.f, Minneapolis, MN 55455, Phone: 612-626-2001, Fax: 612-626-2004, e-mail: pfvdm@cmrr.umn.edu.

We believe that the simplicity and the robustness of this double contrast based approach to address intensity field bias at high field and improve T_1 contrast specificity, together with the capability of simultaneously obtaining angiography maps, advantageously counter balance the potential drawbacks of the technique, mainly a longer acquisition time and a moderate reduction in signal to noise ratio.

Keywords

Bias correction; MP-RAGE; T_1 contrast; Intensity correction; Ultra high field; Adiabatic Inversion; Brain imaging; B_1

Introduction

At high magnetic fields, when the RF wavelength at Larmor frequency is on the order of, or smaller than, the size of an imaged biological target, MR images exhibit undesired intensity variations (often called “intensity field bias”) originating from spatial variations of transmit (B_1^+) and receive (B_1^-) RF coil B_1 profiles. This is the result of complex interactions between radiofrequency waves and electromagnetic properties of lossy dielectric biological tissues (Adriany et al., 2005b; Bottomley and Andrew, 1978; Collins et al., 2002; Glover et al., 1985; Keltner et al., 1991; Van de Moortele et al., 2005; Vaughan et al., 2004; Vaughan et al., 2001; Wiesinger et al., 2004). Most imaging modalities are adversely impacted by these artifacts, including whole brain high resolution T_1-weighted (T_1w) images which are extensively utilized for clinical diagnosis, for gray matter/white matter (GW/WM) segmentation, as well as for coregistration with time series images in functional MRI. 3D-T_1w images are commonly obtained with Magnetization Prepared (MP) sequences, such as 3D-MP Rapid Acquisition Gradient Echo (3D-MPRAGE) (Mugler and Brookman, 1990), where a bulk amount of T_1 contrast comes from an adiabatic non selective inversion pulse, insensitive to B_1^+ variations within a large range of B_1^+ values. However, large signal intensity variations are still present in the images, mostly the result of inhomogeneity in receive RF coil profiles and, to a variable degree, to small flip angle spatial variations.

At lower magnetic fields, such B_1 induced intensity variations (essentially receive RF coil profile, with further amplification due to root sum of square (RSOS) reconstruction) can be efficiently corrected with a variety of post processing approaches (see (Belaroussi et al., 2006; Wang et al., 2005) and references therein), often including low-pass filtering, signal extrapolation and locally adaptive methods. Such algorithms however are not satisfactory at high field where B_1 profiles have much steeper local variations (Van de Moortele et al., 2005; Vaughan et al., 2001; Wiesinger et al., 2004) and cannot be easily approximated or fitted with analytical expressions (e.g. polynomial); consequently, brain segmentation at magnetic fields of 3 Tesla and higher is still a challenging procedure (Belaroussi et al., 2006; Bernstein et al., 2006).

At the acquisition level, 1D shaped and 2D composite RF pulses have been proposed to address RF related inhomogeneity in T_1w 3D-MPRAGE (Deichmann et al., 2000; Deichmann et al., 2002; Deichmann et al., 2004). However, transmit B_1 distortions in the head at 7 Tesla are quite dramatic (Adriany et al., 2005b; Van de Moortele et al., 2005; Vaughan et al., 2001) and could not necessarily be addressed with RF pulse tools that perform well at 3T. Similar correction at 7T would require either B_1 shim or Transmit Sense techniques which, currently, are available only in a few research centers (Adriany et al., 2005b; Katscher et al., 2003; Mao et al., 2006; Setsompop et al., 2006; Vaughan et al., 2001). Other approaches are based on fast B_1 mapping (Yarnykh, 2007) or multi parametric mapping (Warntjes et al., 2007), but they require specific attention and non straightforward

post-processing tools to deal with parametric fitting issues especially when signal to noise ratio (SNR) is low and/or when local tissue conditions depart from the underlying fitting models.

Beside these RF coil related issues, there is a fast growing interest in taking advantage of higher tissue contrasts at higher field. A partial list of these contrasts includes T_1, T_2, T_2* and SWI (Augustinack et al., 2005; Li et al., 2006; Rooney et al., 2007; Thomas et al., 2008), and expectations are that it will be possible with high spatial resolution images at high field to identify some structures or lesions that, so far, cannot be visualized at lower field (Ge et al., 2008). T1w MPRAGE sequences, however, are intrinsically sensitive to Proton Density and T_2* contrast, and T_2* shortening in brain tissues at very high field naturally tends to make the latter bias greater whereas it would be beneficial to investigate separately the contributions of each tissue contrast.

Here[1], we propose a straightforward correction to produce unbiased high resolution T_1w 3D images, relying on two 3D images that are otherwise frequently utilized on clinical scanners: T_1w 3D-MPRAGE and 3D-Gradient Echo (3D-GE). This paper is organized as follows:

- We show that the normalized ratio between two standard 3D images with different contrast provides substantial reduction of intensity field bias by eliminating signal variations induced by B_1-, and yields more accurate T_1 contrast, including at high spatial resolution, by removing T_2* and Proton Density (PD) components, to the cost of a limited loss in Signal to Noise Ratio (SNR).
- We introduce a new sequence where the two contrast acquisitions (MPRAGE and GE) are interleaved, providing a choice between two trade offs: the interleaved sequence which avoids *inter-scan* registration issues, while two separate acquisitions, with a shorter acquisition for each single scan, reduces the risk of *intra-scan* head motion issues.
- We demonstrate that maximum intensity projection (MIP) angiography maps can be derived from the normalized ratio without additional data acquisition.
- We introduce an optional flip angle adjustment scheme allowing for reducing residual bias induced by Transmit B_1 heterogeneity.

Theory

Image Ratio: general principle

The technique presented here involves dividing two images with different contrasts in order to eliminate or reduce most non-T_1 sources of signal intensity variations, while preserving a large fraction of T_1 contrast, as summarized in Table 1. Note that, although we have developed a new sequence interleaving the two image acquisitions, we will describe the principle considering two images acquired separately, which will greatly simplify all subsequent formalism in the manuscript without altering the fundamental principle. The diagram of the sequence is shown in Fig. 1.

[1]Preliminary reports of this work in abstract form include: i) Van de Moortele, P.F., Moeller, S., Ugurbil, K., 2007. Efficient Bias Reduction for High Resolution T1w Imaging in the Human Brain at 7 Tesla. ISMRM Workshop on Advances in High Field MR, Asilomar. ii) Van de Moortele, P.F., Auerbach, E.J., Olman, C., Yacoubd. E., Ugurbil, K., Moeller, S., 2008b. Unbiased High Resolution T1 Weighted Brain Images at High Field with a New Interleaved 3D-MPRAGE/Proton Density GE sequence. Human Brain Mapping 14th Annual Meeting, Sidney. iii) Van de Moortele, P.-F., Auerbach, E.J., Olman, C., Yacoub, E., Ugurbil, K., Moeller, S., 2008a. Which clinical application(s) would best benefit from submillimeter High T1 contrast whole brain images at 7Tesla with simultaneous angiography perfectly coregistered with anatomical images?, Unsolved Problems and Unmet Needs Symposium, ISMRM 14th Annual meeting, Toronto, p. 172.

This approach relies on two fundamental properties: a) the B_1^+ insensitivity of adiabatic inversion over a large range of transmit B_1 magnitude, and b) the reduced amount of T_1 weight in fast GE images obtained with a very small flip angle. Because Proton Density (PD) is their main source of contrast, we will indifferently refer to fast GE images as GE-PD or GE images. The numerator of the proposed image division consists of the signal S_{MP} (MP subscript is for MPRAGE) obtained with a 3D-MPRAGE sequence:

$$S_{MP} \propto \rho \tilde{M}_{MP} \left|B_1^-\right| \sin\left(V \left|B_1^+\right| \gamma\tau\right) e^{-TE/T2^*}, \quad [1]$$

while the denominator consists of the signal S_{GE} (GE subscript for Gradient Echo) obtained with a similar 3D-GE sequence with all matching parameters, but devoid of the inversion RF pulse and associated delays (see Fig. 1):

$$S_{GE} \propto \rho \tilde{M}_{GE} \left|B_1^-\right| \sin\left(V \left|B_1^+\right| \gamma\tau\right) e^{-TE/T2^*} \quad [2]$$

with ρ for proton density, $\mathbf{B}_1^-$ for receive RF coil sensitivity profile, and $M_{MP,GE}$ for the longitudinal magnetization in either MPRAGE or GE-PD. Note that throughout this paper, a tilde sign upon a variable M_{index} indicates magnetization *per unit of proton density* with $M_{index}=\rho_{index}\tilde{M}_{index}$. The flip angle $\alpha=V\left|B_1^+\right|\gamma\tau$ is proportional to transmit B_1 magnitude ($|\mathbf{B}_1^+|$), and γ is the gyromagnetic ratio, τ the equivalent duration of a square pulse, and V a scalar factor (Collins et al., 2002). In the dimensionless ratio image, which we will refer to as Prepared over Non Prepared (P/NP) ratio ([P/NP]=[MPRAGE]/[GE]), the pixel intensity $S_{P/NP}$ can be expressed as:

$$S_{P/NP}=\frac{S_{MP}}{S_{GE}}=\frac{\rho}{\rho}\cdot\frac{\tilde{M}_{MP}}{\tilde{M}_{GE}}\cdot\frac{\left|B_1^-\right|\sin\left(V\left|B_1^+\right|\gamma\tau\right)e^{-TE/T2^*}}{\left|B_1^-\right|\sin\left(V\left|B_1^+\right|\gamma\tau\right)e^{-TE/T2^*}}=\frac{M_{MP}}{M_{GE}} \quad [3]$$

It can be seen that multiple non-T_1 sources of signal intensity variations can be eliminated in $S_{P/NP}$: proton density ρ, receive RF coil sensitivity B_1^-, T_2^* relaxation and $\sin(\alpha)$ (with a small flip angle the latter is approximately proportional to B_1^+). Note that the elimination of T_2^* and PD is only possible when MPRAGE and GE images are acquired at the same spatial resolution (and bandwidth), which is always the case in the present study. A similar approach, mostly dedicated to remove RF coil receive B_1 profile from the data, has also been independently reported (van Gelderen et al., 2006), but GE images were acquired at a lower spatial resolution than MPRAGE and then heavily smoothed (2D kernel 27.5 × 27.5mm^2 FWHM), so that most of the simplifications in Eq. [3] would not apply in that case, as will be discussed and demonstrated later. Here, $S_{P/NP}$ is entirely determined by the longitudinal magnetization per unit of proton density available in each of the two images, and the image ratio technique exploits fundamental differences existing between M_{MP} and M_{GE} with regards to T_1 weight. Indeed, M_{MP} is dominated by a bulk amount of T_1 contrast approximately constant through space resulting from the adiabatic inversion, and this T_1 component, being absent from M_{GE}, is not affected by forming P/NP ratio maps. On the other hand, M_{MP} as well as M_{GE} are non uniformly modulated through space during the fast gradient echo part of the sequences, a direct consequence of spatial heterogeneity of α due to transmit B_1 profile distortions, and they do not have the same functional dependence on α. It will be seen, however, that such residual spatial variations of signal induced by α are limited in P/NP maps.

Longitudinal Magnetization in 3D-MPRAGE

In order to describe the magnetization evolution with 3D-MPRAGE sequences (Mugler and Brookman, 1990) we utilize a formalism similar to the one adopted by Deichmann et al. (Deichmann et al., 2000). The generic sequence (first part of the diagram shown in Fig. 1) includes an adiabatic inversion pulse, an inversion delay TI, a host sequence of duration TA consisting of a fast train of N low flip angle (α) gradient echo (GE) acquisitions spanning through the 1st and 2nd dimension of the 3D k-space with a short repetition time TR, followed by an additional delay TD (Foo et al., 1994), before the next adiabatic inversion, looping through the 3rd dimension of k-space (Mugler and Brookman, 1990). The total duration T_{cycle} between two adiabatic inversion RF pulses is given by $T_{\text{cycle}} = TI + TA + TD$, with $TA = (N\text{-}1)TR$, where N is the number of small flip angle RF pulses within each fast readout echo train and TA the time between the first and the last of those pulses. During the intervals TI and TD, the longitudinal magnetization M relaxes with constant time T_1 towards the value M_0 (magnetization at thermal equilibrium), proportional to proton density ρ. However, during the train of fast GE, the overall longitudinal magnetization evolution can be described as relaxing with a shorter time constant T_1^* (Deichmann et al., 2000; Kaptein et al., 1976), with

$$\frac{1}{T_1^*} = \frac{1}{T_1} - \frac{\ln[\cos[\alpha]]}{TR}, \quad [4]$$

approaching a steady state value M_0^* smaller than M_0 (in Eq. [4], ln is for natural logarithm). Note that if $[\alpha \rightarrow 0]$, then $[T_1^* \rightarrow T_1]$. Here, M_0^* is given by the standard GE steady state equation:

$$M_0^* = M_0 \frac{1 - E_{T_1}^{TR}}{1 - \cos[\alpha] E_{T_1}^{TR}}, \quad [5]$$

with $E_{T_1}^{TR} = e^{-TR/T_1}$ (in this paper any expression in the form of E_V^U stands for $E_V^U = e^{-U/V}$).

Assuming that T_1 contrast is mostly determined at the k-space origin (Deichmann et al., 2000), and considering a linear phase encoding (LPE) scheme[2] along the fast readout echo train, we express the MPRAGE longitudinal magnetization at the sampling time $TS_{\text{LPE}} = TI + TA/2$:

$$\frac{M_{\text{LPE}}}{M_0} = \frac{\left[1 - E_{T_1}^{TR}\right]\left[1 - E_{2T_1^*}^{TA}\right]}{1 - E_{T_1^*}^{TR}} + E_{2T_1^*}^{TA} \left[\frac{1 - E_{T_1}^{TI} - \xi \left[E_{T_1}^{TI} \left[1 - E_{T_1}^{TD}\right] + \frac{E_{T_1}^{TI} E_{T_1}^{TD} \left[1 - E_{T_1^*}^{TA}\right]\left[1 - E_{T_1}^{TR}\right]}{1 - E_{T_1^*}^{TR}} \right]}{1 + \xi E_{T_1}^{TI} E_{T_1^*}^{TA} E_{T_1}^{TD}} \right] \quad [6]$$

where ξ, efficiency of the inversion pulse (Gelman et al., 2001), determines the fraction of longitudinal magnetization actually inverted [$-1 \le \xi \le 1$, ideally $\xi = 1$]. This is equivalent to

[2]The exact time when the k-space origin is sampled (TS) is given by $TI + (N/2 \pm \text{mod}(N,2)) * TR$ where mod(N,2) is the residual after dividing N by 2. However, for simplicity we consider here $TS \approx TI + TA/2$ because $TR \ll TS$. Also, in case of Partial Fourier acquisition, the actual sampling time of the k-space origin is shifted away from the middle of TA.

writing $\xi = -\cos\theta$, with θ the effective flip angle achieved along the Z axis at the end of the inversion pulse [ideally $\theta = 180°$].

One can note that in Eq. [6], if the small flip angle α approaches zero, then T_1^* approaches T_1, the problem reducing then to a simple mono exponential case. For illustration, if we also assume $TD \gg T_1$ then after Eq. [6]:

$$\lim_{\alpha \to 0} M_{\mathrm{LPE}} = M_0 \left(1 - (1+\xi)\, E_{T_1}^{TS_{\mathrm{LPE}}}\right). \quad [7]$$

Within this extreme approximation, ξ and TS_{LPE} would be the only sequence parameters impacting T_1-weight and, assuming that $|B_1^+|$ is above adiabatic threshold, full inversion would be obtained irrespective of B_1^+ inhomogeneities [$\xi = 1$], reducing further the expression into:

$$\lim_{\alpha \to 0} M_{\mathrm{LPE}} = M_0 \left(1 - 2E_{T_1}^{TS_{\mathrm{LPE}}}\right). \quad [8]$$

In the interleaved version, a second train of fast GE (followed by an optional delay $TD2$ which typically is null) is inserted between TD and the next inversion pulse, with the kspace center of the GE image sampled at TI + TA + TD + TA/2 in the case of linear phase encoding without partial Fourier acquisition. Although the same fundamental principles apply for both separate and interleaved acquisition, we did not include in this manuscript the formalism of the interleaved version which results in a fairly long expression. The main difference compared with separate acquisitions is that the delay TD now also determines how close to steady state the longitudinal magnetization is at the beginning of the second train of fast gradient echo (GE image). As a result, if the delay ($TI + TA + TD$) is not long enough with regards to T_1, the GE image may carry a significant amount of T_1 contrast.

Noise propagation

In this section we only address the Signal to Noise Ratio (SNR) available in the ratio images; residual signal intensity variations and impact on tissue contrast are discussed elsewhere. The noise propagation in the ratio x of two variables u and v, with $x = u/v$, can be expressed as (Bevington, 1969):

$$\frac{\sigma_x^2}{x^2} = \frac{\sigma_v^2}{v^2} + \frac{\sigma_u^2}{u^2} + 2uv\sigma_u\sigma_v \quad [9]$$

(σ is the standard deviation). With same noise level in MPRAGE and GE-PD images, i.e. $\sigma_{\mathrm{IM}} = \sigma_{\mathrm{MPRAGE}} = \sigma_{\mathrm{GE}}$, and assuming that noise in MPRAGE signal (S_{MP}) and GE-PD signal (S_{GE}) are uncorrelated, i.e. $\sigma_u\sigma_v = 0$, we can write:

$$\frac{\sigma_{\mathrm{P/NP}}^2}{S_{\mathrm{P/NP}}^2} = \sigma_{\mathrm{IM}}^2 \left[\frac{1}{S_{\mathrm{MP}}^2} + \frac{1}{S_{\mathrm{GE}}^2}\right]. \quad [10]$$

As we are mostly interested in comparing SNR in P/NP ($SNR_{\mathrm{P/NP}}$) and in MPRAGE (SNR_{MP}) this can be expressed as:

$$SNR_{\mathrm{P/NP}} = \frac{SNR_{\mathrm{MP}}}{\sqrt{1+S^2_{\mathrm{P/NP}}}}. \quad [11]$$

With the technique presented here, $S_{\mathrm{P/NP}}$ was typically around 0.65 or less in the white matter and around 0.35 or less in the gray matter with our acquisition parameters (with different sequence parameters different $S_{\mathrm{P/NP}}$ values could be found; however, $S_{\mathrm{P/NP}}$ was in this range for a variety of parameter sets at 7T). Compared with the source MPRAGE images, this corresponds to a loss in SNR of only ~6% in gray matter and ~16% in white matter (see Fig. 2). Fortunately, it can be seen that the largest percentage of SNR loss, although still moderate (16%), occurs for the largest initial SNR (white matter), indicating that the present ratio technique will have only a limited impact on the overall SNR.

Impact of image division on WM/GM contrast

The question addressed in this section is the impact of dividing an MPRAGE image with a GE-PD image on white matter/gray matter contrast, with pre-existing contrast in MPRAGE taken as a reference. For this purpose, we assume all acquisition parameters identical for white and gray matter, including α and B_1^-, and we also ignore differences in WM/GM T_2^*'s whose relative weight depend on which particular TE is chosen. Note that we do not attempt to address here T_1 contrast issues and Point Spread Function (PSF) optimization in MPRAGE sequences, which have been extensively investigated elsewhere (Deichmann and Haase, 1992; Foo et al., 1994; Haase, 1990; Mugler and Brookman, 1990).

The WM/GM contrast in MPRAGE images and in P/NP maps can be expressed as (see Appendix 1):

$$C^{W/G}_{\mathrm{MP}} = \frac{1 - D^{G/W}_{\mathrm{MP}}}{1+D^{G/W}_{\mathrm{MP}}}, \quad [12]$$

and

$$C^{W/G}_{\mathrm{P/NP}} = \frac{1 - \lambda D^{G/W}_{\mathrm{MP}}}{1+\lambda D^{G/W}_{\mathrm{MP}}}, \quad [13]$$

with $D^{G/W}_{\mathrm{MP}} = \frac{S^{G}_{\mathrm{MP}}}{S^{W}_{\mathrm{MP}}}$. The value of λ is entirely determined by the GE-PD image (as long as the same value for α is utilized in MPRAGE and GE-PE) and can be expressed as (see Appendix 1 and Eq. [2]):

$$\lambda = \frac{\rho^W}{\rho^G} \cdot \frac{\tilde{M}^{*W}_0}{\tilde{M}^{*G}_0}. \quad [14]$$

Eq. [13] shows that the WM/GM contrast in Ratio Images decreases with λ>1, increases with λ<1 and is unaltered with λ=l. It is also immediately apparent with Eq. [14] that two GE-PD image components act in opposite directions: the ratio of proton density tends to increase T_1 contrast [$\rho^{\mathrm{W}} \div \rho^{\mathrm{G}} \approx 0.8$], whereas steady state longitudinal magnetization per unit of PD tends to decrease T_1 contrast [$\tilde{M}^{*W}_0 > \tilde{M}^{*G}_0$]. Very importantly, a simple visual

inspection of the GE-PD images is sufficient to determine if λ is smaller than one (GM brighter than WM, PD contrast greater than T_1 contrast) or bigger than one (WM brighter than GM, T_1 contrast greater than PD contrast). With a small flip angle and a short TR, λ is typically smaller than one, thus overall WM/GM contrast is actually *greater* in the ratio images than in MPRAGE images because the gain in WM/GM contrast obtained by removing PD contrast is larger than the limited loss in T_1 contrast due to the residual T_1 weight existing in GE-PD images. This increase in WM/GM contrast also reduces the loss in Contrast to Noise Ratio (CNR) in the ratio images despite a lower SNR. (CNR can even increase in ratio images depending on the acquisition parameters). The ratio between the WM/GM contrast in Ratio Images and the WM/GM contrast in MPRAGE can be written as:

$$\frac{C^{W/G}_{\mathrm{RATIO}}}{C^{W/G}_{\mathrm{MP}}} = \frac{1-\lambda D^{G/W}_{\mathrm{MP}}}{1+\lambda D^{G/W}_{\mathrm{MP}}} \cdot \frac{1+D^{G/W}_{\mathrm{MP}}}{1-D^{G/W}_{\mathrm{MP}}} \quad [15]$$

Material and methods

Healthy volunteers who had signed a written consent form approved by the Institutional Review Board of the University of Minnesota were imaged at 7 Tesla. The images obtained in separate acquisitions were obtained with standard sequences available on the scanners (MPRAGE and GE-PD). The interleaved sequence (Van de Moortele et al., 2008b) was developed in house for the 7T Siemens console. Because this study is primarily concerned with the impact of forming the ratio between MPRAGE and GE-PD images, rather than with optimizing each individual acquisition, we utilized a variety of existing protocols without attempting to modify their T_1 contrast characteristics. For all 3D-MPRAGE images described below, corresponding 3D-GE images acquired separately were obtained with all parameters identical but without inversion pulse and with TI and TD set to zero. One exception concerns the small flip angle and will be discussed later.

Note that the inversion time TI as defined on the Siemens console (TI_{Siemens}) refers to the time when the center of the k-space is sampled along the 2nd dimension. In the present manuscript TI actually refers, as suggested elsewhere (Deichmann et al., 2000), to the time when the train of fast GE readouts begins. Thus, with linear phase encoding and in the absence of partial Fourier reconstruction: $TI_{\mathrm{Siemens}} = TI + TA/2$.

7 Tesla experiments

Imaging experiments were performed with a 7 Tesla magnet (Magnex Scientific, UK) driven with a Siemens console (Erlangen, Germany). A 16-channel transmit/receive head array coil, as described in (Adriany et al., 2005a; Adriany et al., 2005b) was used for both RF-transmit and signal-receive operations in whole brain imaging experiments. Additional data were obtained in the occipital lobe with another RF coil setup which has been described in details elsewhere (Pfeuffer et al., 2002): briefly, signal reception was obtained with a quadrature RF coil made out of two partially overlapping loops of 6 cm diameters, while RF transmission was produced with a large half volume quadrature surface coil ($18 \times 12\mathrm{cm}^2$ pair). Multiple sets of parameters were used to acquire 3D-MPRAGE and 3D-GE images, either as separate acquisitions or with the interleaved sequence, and the corresponding details will be found in the figure captions. Note that in all experiments involving acceleration with GRAPPA the number of auto calibration lines was set to 24.

Ratio Images and thresholding

MPRAGE and GE-PD magnitude images were exported from the acquisition console in DICOM format, explicitly excluding any intensity correction filter during image reconstruction at the console. P/NP ratio maps were then obtained by directly dividing MPRAGE images with corresponding GE-PD images. In order to limit meaningless high pixel intensity in pixels divided with noise, a binary mask was defined based on SNR thresholding in GE images. The threshold value was determined manually in order to exclude background noise from the volume of interest. Pixels excluded from this mask were set to zero in the Ratio Images. In order to investigate the impact of using a smoothed reference image we also generated a smoothed reference image by convolving the high resolution GE with a 27.5×27.5 mm^2 FWHM Gaussian kernel, as described in (van Gelderen et al., 2006).

Motion correction

With data sets obtained in two separate acquisitions *inter-scan* head motion can occur, translating in edge artifacts in ratio images. In such cases we utilized the FLIRT toolbox (Jenkinson et al., 2002) in the FSL package (Smith et al., 2004) in order to realign the 3D-MPRAGE image onto the 3D-GE image.

Brain segmentation

Based on the normalized ratio images, whole brain segmentation as well as white and gray matter surface rendering can now be obtained as a routine procedure in our center at 7 Tesla using the SurfRelax package (Larsson, 2001). Those specific developments are beyond the scope of this paper and will be detailed elsewhere (Olman et al., 2007). One significant result will, however, be shown in the present manuscript demonstrating successful brain segmentation at 7 Tesla based on high spatial resolution ratio images.

Maximum Intensity Projection Angiography

Gray matter, white matter and CSF inherently exhibit higher signal intensity in low flip angle 3D-GE than in 3D-MPRAGE images, so that their ratio value is always smaller than one (except in locations where B_1^+ is so weak that inversion pulses do not reach adiabatic conditions). This is not the case for flowing blood. Indeed, we observed that the net signal of flowing blood is greater in 3D-MPRAGE than in 3D-GE images, resulting in values greater than unity in P/PN ratio images for voxels located in vessels. As a result, with an appropriate threshold one can isolate signals originating from vessels in the ratio images, and Maximum Intensity Projection (MIP) maps (Laub, 1990) can then be utilized to visualize those vessels. The short T_1 of fat in skin tissues, however, also produce confounding bright signals, a well known issue in MIP images which can be overcome by excluding the corresponding pixel from the analysis. Angiograms were produced with the following steps. First, MPRAGE and GE images were interpolated at twice the acquisition spatial resolution before forming NP/P ratio images. Then skin and skull were removed from the ratio images using morphomathematical tools (erosion/dilation) from a 3D toolbox (SDC Information Systems, Naperville, IL) written for matlab. A minimum intensity threshold was then manually adjusted in order to retain vessels (brighter pixels) while excluding tissues (darker pixels), and the resulting angiography was visualized as MIP maps along axial, sagittal and coronal projections. All computations were performed in Matlab (The Mathworks, Inc.).

Results

Intensity field bias correction

Typical results obtained at 7 Tesla are shown in Fig. 3: intensity variations in MPRAGE images are such that the gray scale cannot be adjusted to accommodate all gray values through brain tissues, or tissue contrast would be lost. One can see that similar variations of signal intensity, on a large spatial scale and with large amplitude, affect both MPRAGE and GE-PD images, whereas P/NP ratio images are much more homogeneous, still preserving excellent gray/white matter contrast. White arrows in the figure are pointing towards areas where signal intensity is either too high or too low when trying to manage a unique gray scale windowing for the whole brain in MPRAGE or GE images. The corresponding areas are within a homogeneous range of gray scale in P/NP images. Note also that the technique performs well from the vertex to the lowest part of the brain. While those images were obtained with a small flip angle of 3°, they do not suffer from a poor SNR, indicating that spatial resolution can be increased further with this approach at high field, as will be shown later with the interleaved sequence.

Initially designed for whole brain T_1w imaging at 7T, the ratio technique also proved very efficient with surface RF coils. This is shown in Fig. 4 where 3D MPRAGE images were obtained at 7 Tesla with a half volume RF transmit coil and a 2-loop quadrature receive coil. Such surface coil data typically provide images with steep signal decay as a function of distance to the coil and naturally suffer a loss in SNR when compared with an array of receive coil elements sampled on different receive channels (Roemer et al., 1990). The ratio technique, instead of traditional images with constant thermal noise and large intensity variations, inherently provides images with constant average signal intensity whereas local noise levels are rescaled accordingly. In other words, parts of the brain that are extremely dark in MPRAGE images, such as the cerebellum and central structures in this particular case, have intrinsically very low SNR and a single gray scale display would not accommodate more than a small fraction of the imaged tissues. In P/NP ratio images (Fig. 4), all areas are now equally visible with high T_1 contrast. As expected, the noise in P/NP images is much more visible in low SNR areas. It is important to distinguish such increases in noise visibility from actual *losses* in SNR which, as was discussed in the Theory section, are actually very moderate when forming P/NP ratio images. A source of SNR reduction compared with Fig. 3 is due to using a single receive channel coil versus a 16 receive channels coil, together with lower amount of collected data (smaller matrix size).

Head motion and interleaved sequence

Head motion between two separately acquired scans can naturally be a serious issue as illustrated in Fig. 5 for images obtained with a healthy volunteer. Even limited motion is sufficient to produce evident edge artifacts in the P/NP ratio images which could jeopardize tissue classification procedures. As can be seen in the same figure, it was possible to successfully realign 3D-MPRAGE onto 3D-GE utilizing the standard FLIRT package and eliminate any noticeable artifacts in the ratio obtained with realigned data. This registration, however, typically comes at the price of a certain degree of blurring often induced by the interpolation filter. Naturally, using a higher spatial resolution makes realignment issues even more challenging. The interleaved sequence that we have developed in order to address this issue is virtually insensitive to *inter-scan* head motion (except for brief jumps in head position shorter than T_{cycle}), as equivalent k-space lines in MPRAGE and GE are acquired with almost same head position even when head position slowly moves throughout the course of the acquisition. It should be noted that, due to a longer single scan time, the interleaved sequence increases the risk of *intra-scan* head motion artifacts. Nevertheless, standard segmentation algorithm performed very well even on ratio images obtained with

the interleaved sequence, including at a spatial resolution of 0.27 mm^3 and without applying any spatial filtering, as illustrated in Fig. 6. Because the current technique provides both unbiased P/NP and uncorrected T_1w 3D MPRAGE images, it is straightforward to overlay parametric maps calculated with P/NP ratio onto MPRAGE images, as shown for gray/white matter segmentation (see yellow contours). One can note that, besides cerebral tissues, very large signal intensity variations in skin and skull are remarkably corrected, making skull stripping procedures easier.

Angiogram

Another advantage of removing intensity non-uniformities is to improve vessel visualization with high resolution isotropic MIP angiograms (Fig. 7), helping to identify blood vessels, which can constitute a valuable information for functional MRI analysis as well as for anatomical structural imaging. The angiograms shown in Fig. 7 were obtained by forming Maximum Intensity Projection maps along the X, Y and Z axes, after removing outer non-cerebral structures from the data set shown in Fig. 6. Note that, whereas segmentation was obtained without spatial smoothing (Fig. 6), 3D-GE images (but not 3D-MPRAGE) were spatially smoothed before forming ratio images utilized to produce angiograms. We found that filtering GE images with a 3D-gaussian convolution kernel with a FWHM of ~1.5mm was a good tradeoff allowing for improving local SNR while preserving vessel structure identification. We hypothesize that the benefit of this filter is in part due to the fact that the blood signal is *decreased* in GE images compared with MPRAGE, a less favorable situation for noise propagation because GE images are the denominator of the ratio.

Smoothed vs. Unfiltered GE reference: Impact on Brain Structures at High Spatial Resolution

Because of the inherent sensitivity of T1w MPRAGE images to Proton Density and T_2* contrast we hypothesized that the appearance of some brain structures may be contaminated with non-T_1 components. Such non-T_1 contributing patterns, however, are expected to reflect small brain anatomical structures, thus requiring a high spatial resolution reference image to be corrected for. Opposite to this case, receive B1 profiles typically have much smoother spatial patterns and should be successfully removed with a low spatial resolution reference image. To verify these hypotheses high resolution data were obtained with the interleaved sequence, and the MPRAGE images were divided either with the unfiltered GE image (same spatial resolution) or with the GE image smoothed with a 27 × 27.5mm^2 Gaussian kernel, as described in (van Gelderen et al., 2006). A few observations can be made about the corresponding results shown in Fig. 8. First of all, unwanted slow spatial variations of signal (mostly corresponding to receive B1 profiles) clearly present in original MPRAGE images (fourth column), were very efficiently removed with both the smoothed (first column) and the unfiltered (second column) GE image, resulting in corrected images shown in the third and fifth column, respectively. On the other hand, when comparing MPRAGE image with MPRAGE/Filtered GE we could not identify high spatial frequency alteration between the two images, which also was expected.

However, the division of the MPRAGE image with the unfiltered high resolution GE reference was capable of unveiling some cerebral structures which were difficult to identify in MPRAGE images (compare the white box contents in the fourth and fifth columns), and these anatomical structures clearly include very high spatial frequency components. This is supported by a comparison between the first and the second rows, which are showing closely matching axial views extracted from two data sets acquired with isotropic 0.51mm^3 voxel size (first row) and isotropic 0.3mm^3 voxel size (second row). These two data sets (each consisting in MPRAGE + GE 3D images) were acquired with the interleaved sequence in the same volunteer within the same session. In the second row, the higher spatial

resolution naturally results in smaller and more numerous structural details being identified in MPRAGE as well as in GE images. Interestingly, this higher spatial resolution also results in smaller and more numerous structural details being unveiled in the MPRAGE/GE image whereas the low spatial signal variations (receive B1) were removed with apparently equal success at both spatial resolutions and with either GE or Filtered GE. The third and fourth rows in Fig. 8 are showing coronal views of a data set obtained in another volunteer with isotropic 0.3mm^3 voxel size. Again, inside the white box in the third row some small structures are better identified in MPRAGE/GE compared with MPRAGE.

We assume that the aforementioned unveiled anatomical structures may be due in a large part to the removal of Proton Density which typically cancels a fraction of T1 contrast between gray and white matter in MPRAGE images. However, shorter T_2* at higher field can yield losses of signals, especially close to vascular structures, and it may be difficult to determine with certainty the origin of such small signal defects in MPRAGE images. In the fourth row of Fig. 8, the two white arrows point towards small dark spots in GE images, each surrounded with two small bright spots along the Z direction, suggestive of typical susceptibility effects induced by small vessels. Because T2* contribution are the same in MPRAGE and GE images, one would expect most of this aspect to be removed when forming the ratio between these two images. Indeed, these vessel induced patterns essentially disappeared in MPRAGE/GE (fifth column), while they were left intact in MPRAGE/Filtered GE.

When a longer segment of a vessel, rather than just a normal section, is captured within a slice, the pattern of resulting signal losses can become more complex and more difficult to interpret. Such a situation is illustrated in Fig. 9 showing, on three rows, three contiguous parasagittal views extracted from an isotropic 0.3mm^3 data set (interleaved acquisition). The pattern of approximately horizontal dark and bright lines enclosed between the brackets, present in both MPRAGE and GE, is considerably attenuated in the ratio MPRAGE/Filtered GE, with smoother and better identified tissue borders.

Besides blood vessels, some brain tissues also have shorter T_2*, which in MPRAGE images translates in lower signal intensity that cannot be differentiated from actual T_1 contrast, which again affects T_1 contrast specificity. Note that here, removing T_2* components from MPRAGE images should result in an apparent *decrease* in tissue contrast. This mechanism is likely to explain, in Fig. 9, the lower visibility of the structure labeled ‘iii’ in MPRAGE/GE compared with MPRAGE. By contrast, both structures labeled ‘i’ and ‘ii’ appear with increased contrast and sharper edges in MPRAGE/GE than in MPRAGE, suggesting the absence of significant T_2* component in the two latter structures.

Residual Transmit B1 induced bias

It is known that transmit B_1 profiles becomes significantly heterogeneous at 7T (Collins et al., 2002; Van de Moortele et al., 2005; Vaughan et al., 2001). As a consequence, larger residual signal variations are expected in P/NP maps at 7T due to the contribution of a more heterogeneous a. In order to apprehend better this phenomenon we have simulated, based on Eqs. [5] and [6], the impact of a variations on P/NP ratio values for different values of T_1, utilizing same acquisition parameters as in Fig. 3. As can be seen in Fig. 10A, our simulations predict that variations in a can have a significant impact on signal intensity in P/NP, (other reports had suggested that the impact of transmit B_1 profile would rather disappear in ratio images (van Gelderen et al., 2006)). This plot also reminds that above a certain threshold for a, T_1 contrast reduces when a increases, a feature which is known for MPRAGE sequences utilizing linear phase encoding (Deichmann et al., 2000). Strikingly, as shown in Fig. 10B, simulations suggest that simply utilizing a flip angle in MPRAGE larger than in 3D-GE may considerably attenuate the sensitivity of P/NP to a variations,

potentially providing an additional tool to obtain more regular P/NP maps at very high field. A preliminary experimental verification can be seen Fig. 11, showing three different ratio images obtained with a volunteer for whom, within a same session at 7 Tesla, both MPRAGE and GE images had been acquired two times, first with a nominal flip angle of 3° and then with a nominal flip angle of 6°. In Fig. 11, the ratio MPRAGE[α=6°]/GE[α=6°] clearly exhibits significant residual intensity bias. To interpret the patterns in those images, it is important to remember that receive B_1 profile obtained when summing multiple receive RF coil sources (16 channels here) results in brighter intensity close to the coils (i.e. in the periphery of the brain), and that this receive component is expected to be entirely absent in ratio images, independently of a (see [3]). In Fig. 11, however, spatial patterns of residual brighter intensity fundamentally differ from the sum of receive B_1 profiles. Here, in an axial view the brighter signal area includes the center of the brain and is diagonally stretched towards the periphery, and in a coronal view the brighter component concerns the central part of the brain. Those patterns are highly consistent with B_1^+ profiles previously measured at 7T with transceiver array coils similar to the one utilized here (Adriany et al., 2005b) or with TEM head RF coils (Vaughan et al., 2001). Those brighter areas are considerably attenuated when utilizing a smaller value for a in both MPRAGE and GE, as seen in the ratio image MPRAGE[α=3°]/GE[α=3°]. Interestingly, dividing the larger flip angle MPRAGE[α=6°] with the smaller flip angle GE[α=3°] reduces even further the residual transmit B_1 induced intensity variations, consistent with the prediction plot shown in Fig. 10.

Adiabatic inversion

The residual transmit B_1 profiles described above are related with the small excitation flip angle a, which is approximately proportional to $|B_1^+|$. Adiabatic inversion, however, is expected to be uniform through space, except when $|B_1^+|$ falls below a minimum threshold. The subsequent local lack of inversion naturally yields a loss in T_1 contrast in MPRAGE images, but a weak $|B_1^+|$ also yields a very small flip angle so that local SNR can be very low, making it difficult to determine if a local dark area rather results from RF coil issues or from anatomical features. As can be seen in Fig. 12, such failures are be easier to identify in P/NP images under the form of a local spot brighter then gray and white matter areas (see details in Fig. 12 caption). Because with the present technique MPRAGE and GE images are available as well, one can easily verify that such bright area in P/NP corresponds to a dark area in GE images and to a loss of local contrast in MPRAGE images. Besides B_1^+ profiles, other well known sources of inversion failure, especially with non selective inversion pulses, include areas with local susceptibility induced resonance offsets larger than half the bandwidth of the inversion pulse. In such locations, and in the absence of local B_1^+ defect, the lack of T1 contrast yields high signal intensity in MPRAGE images, which translates in the ratio images in areas brighter than gray and white matter (data not shown). Because such artifacts occur in the vicinity of air/bone/tissue interfaces they are usually easily identified. However, here again a simple visual inspection of the 3 available images with different contrasts allows for an immediate verification.

Discussion

Utilizing the ratio of two standard MR images proves to be a very efficient technique to eliminate the receive coil profile from T1w MPRAGE images at 7Tesla, with a volume or a surface coil. This is expected to greatly facilitate whole brain tissue segmentation as well as co-registration between imaging sessions obtained at different times, using different RF coils and on different scanners. This might be especially advantageous in follow-up studies. The current technique directly relies on unmodified, gold standard T_1w images, which are available to the clinician in addition to the unbiased T_1w images. In addition to removing

signal intensity variations due to coil sensitivities, which are common targets in post processing field bias correction techniques, the current approach also removes T_2* and proton-density contributions, providing a more accurate T_1 contrast; furthermore, Maximum Intensity Projection angiograms can be generated without additional acquisition.

T2* and Proton Density contrast removal

At low fields, transverse relaxation in brain tissues is very limited during fast GE acquisition because tissue T_2*'s are much longer than TE. At high field, however, this assumption might not always be valid due to short T_2*'s and due to even shorter T_2*'s in the vicinity of small structures surrounded with steep B_0 gradients (e.g. small veins). At 7T, for example, T_2* values have been reported as ~25-35ms in white and gray (cortical) matter, ~20ms in Caudate, ~16ms in Putamen, and ~13ms in vessels (Li et al., 2006; Peters et al., 2007; Yacoub et al., 2001). Keeping a short TE at very high spatial resolution in order to limit T_2* weight is doable to a certain extent but is constrained by hardware and safety limitations (maximum gradient strength, slew rate) and, especially at high field, tends to significantly increase gradient coil acoustic noise. Furthermore, it has been shown that T_1 distribution through the gray matter is significantly more distributed at 7T than at lower field, potentially carrying more information (Rooney et al., 2007). For those reasons it is desirable to remove T_2* components from T_1w images obtained at high field.

Although Proton Density and T_1 values have been reported as highly correlated in the brain (Gelman et al., 2001; Just and Thelen, 1988), they yield opposite contrasts in T_1w images, which have inherently some contrast loss due to PD. This loss in T_1 contrast is typically recovered in P/NP images (with the interleaved sequence this requires $TI + TA + TD$ to be long enough in order to limit T_1 contrast in GE images).

Our experimental results confirm the benefit of removing T_2* and PD components from T_1 MPRAGE images, resulting in better brain structure visualization at a small spatial scale as well in some restitution of signal in short T_2* location. Our results also point towards additional potentiality in utilizing the original T_1w MPRAGE and GE images in conjunction with the ratio images.

Residual transmit B_1 induced bias

The simplified mathematical model in Eq. [5] and [6] indicates that utilizing very small values for α at 7 Tesla (such as 3°) should result in lower amounts of residual transmit B_1 induced signal variations in P/NP ratio (see Fig. 10). Given the higher SNR available at higher field, and considering that T_1 contrast is better preserved with smaller values of α, this suggests that very small flip angles (such as 3°) can advantageously be used at very high field (see Fig. 3).

In general, within the range of parameters used in the present study, we found P/NP maps acceptably uniform when utilizing the same α value for MPRAGE and GE, as long as the nominal value for α did not exceed about 5°. Our simulations, however, predicted further improvements by utilizing a larger flip angle in MPRAGE than in GE images (Fig. 10), which is supported by additional experimental data acquired with two different values for α (Fig. 11). Naturally, using a smaller value for α in both MPRAGE and GE means a lower SNR in both images. The two different flip angle approach reduces this SNR penalty by increasing signal intensity in MPRAGE, as long as α is within limits of preserving a T_1 contrast predominantly induced by the inversion pulse (Deichmann et al., 2000). In the particular data shown in Fig. 11, the residual transmit bias observed with α=6° was somewhat more pronounced than in other similar data sets. However, our nominal flip angles at 7T were determined with standard calibration routines delivered with the console,

that are not reliable at ultra high field as demonstrated by Collins et al. (Collins and Smith, 2001), and depend among other things on which part of the brain (high or low transmit B_1) is at the magnet isocenter during the calibration. It is thus possible that the actual average flip angles were somewhat higher than 3° and 6° in this case, but a similar trend (reduced transmit residuals with smaller α value, and further improvement with α [MPRAGE] larger than α [GE]) was consistently found in multiple data sets (not shown). The range of transmit B1 variations through the brain greatly depends on RF coil design which, together with new technologies such as B1 Shimming, could mitigate this issue in the future. However, being able to improve further P/NP quality by choosing two values for α offers the advantage of a straightforward implementation, and optimum values could be calculated on the fly based on acquisition parameters.

Adiabatic inversion

Whereas at lower field RF excitation is most of the time obtained with a large body RF coil, most neuroimaging experiments at 7T utilize head RF coils which are sometimes closely fitting to the head (Adriany et al., 2005a). Relative phase maladjustments between transmit channels can then result in weak transmit B_1 amplitude in some areas (Adriany et al., 2005b), a direct consequence of large B_1 distortion at high field (Van de Moortele et al., 2005). Although specific solutions (RF coil design, B_1 shim, Transmit SENSE, etc.) are under active development, they are not yet available in most imaging centers. Thus, it is important to be able to identify potential local failure in adiabatic inversion at 7 Tesla. We show here (see Fig. 12) that a local spot of weak $|B_1^+|$, below adiabatic threshold, typically translates into an abnormally *bright* areas in P/NP images that are easier to identify than in MPRAGE images. This is because, with an incomplete inversion, the longitudinal magnetization is much closer to thermal equilibrium at the sampling time, whereas the low signal intensity term due to the small flip angle affects both the T_1w and reference images, and hence for the most part cancels when forming the ratio. It will be important to evaluate whether this artifact identification criterion would be reliable in the case of tissues alterations under pathological conditions.

Acquisition strategy: scan time, SNR, spatial resolution, head motion

One noticeable limitation of our technique is the additional time required for acquiring a 3D-GE reference image (with an acquisition time typically between half and three quarter of that for 3D-MPRAGE), with resulting SNR in unbiased T_1w images rather moderately lower than in 3D-MPRAGE. This would evidently not be an efficient strategy if SNR was a prominent target. In the current study, however, our main goal was not to improve SNR. Rather, we aimed to demonstrate a technique which takes advantage of inherently high SNR and CNR at high field in order to produce high resolution images with high T_1 contrast specificity, devoid of T_2* and Proton Density contrast and of the large signal variations due to receive coil profiles. For this reason, the results presented here were not evaluated in term of SNR efficiency per unit of time, which actually rather decreases in P/NP compared with MPRAGE alone. Our main criterions rather were to succeed in getting routine tissue classification through the whole brain despite severe B_1 distortion, in demonstrating the benefits of higher T_1 specificity to identify brain structures at high resolution, in handling *inter-scan* head motion issues, and in addressing residual transmit B_1 bias. We verified that our technique could easily be implemented for a variety of existing T_1-weighted MPRAGE protocols (a concern expressed by multiple users). We also verified that, even in much noisier conditions than standard isotropic cubic millimeter resolution, tissue brain segmentation was successfully obtained, even without any spatial filtering (see Fig. 6).

Note that at low spatial resolution, T_{cycle} can be fairly short in standard (non interleaved) $T_{1\text{w}}$ MPRAGE acquisitions. As a result, a significant delay TD would be required to use the

interleaved version in order to be close to steady state for the GE acquisition, yielding a low temporal efficiency. This is not the case at higher spatial resolution where TA tends to be significantly longer so that only a relatively short delay TD is sufficient. In the later case, the interleaved acquisition is not significantly longer than the sum of two separate acquisitions. In the present study the additional scan time needed to acquire isotropic cubic millimeter resolution whole brain 3D-GE images at 7 Tesla varied from 2min36s (out of a total of 7min30s for two interleaved images, see Fig. 12) up to 5min45s (separate acquisitions, Fig. 2). For the higher resolution data sets (0.27mm3), the GE image took 5 minutes (out of a total of 14min12s for two interleave images). We found that those additional scan times were not a problem with healthy volunteers; this would naturally be seen differently with patients. Additional investigation will, however, be needed to optimize tradeoffs between spatial resolution, SNR, CNR and acquisition time which depend on multiple acquisition parameters (T_{cycle}, TR, TE, bandwidth, TI, TD, TA, partial Fourier and parallel imaging acceleration)

Regarding spatial resolution for GE images, another similar approach successfully utilizing a GE reference in order to correct T_1w MPRAGE images for receive B1 profile has been independently demonstrated by others at 7T (van Gelderen et al., 2006). However, GE images were acquired at a lower resolution than MPRAGE and then heavily spatially smoothed. This is perfectly suitable for solely removing receive B_1 induced intensity field bias, in which case low resolution GE images can indeed be acquired in a short time to efficiently correct for receive B1 bias (scan time = 1min in the referenced work), as shown in our results as well. (it should be reminded that utilizing large smoothing convolution filters still requires the use of specific algorithms in order avoid significant artifacts at the periphery of the brain).

We find, however, considerable interests in acquiring both images at matching spatial resolution, worth in our view the cost of up to 5 minutes of scan time. The resulting high resolution images with high T_1 contrast specificity (without T_2*, PD and B1 contribution) can be used for applications such as clinical diagnosis, cortical thickness mapping or brain segmentation, as well as to produce angiograms.

Angiograms

We see the MIP angiograms as a very significant addition. Because they are directly derived from the ratio, they should allow for unambiguous identification of vessels location with regards to brain structures without resampling or co-registration error. A remarkable characteristic was the clear and homogeneous separation between vessels and cerebral tissues through the whole brain, which we attributed to the normalizing ratio. Indeed, the vessel information (bright pixels) is present in the MPRAGE images and as such could be in principle directly extracted from these data without forming the ratio images. With this approach, however, it would be impossible to obtain whole brain angiograms in a single step MIP process, because in large areas vessels would be obscured by brain tissues exhibiting larger signal intensity. In the ratio images, a simple intensity threshold (after removal of skin and skull) was sufficient to produce through the whole brain MIP angiograms with almost no signal visible in the background. Optimizing those angiograms while preserving high quality, low bias T_1w tissue images will be an important target of our future investigations with this technique. It should be noted that removing T_2* and PD contrasts is not expected to have an impact as significant for the angiograms as for the T_1-weighted images.

Low SNR mask

When dividing an image with another one, pixels that have only noise or very low SNR in the denominator image generate very high, meaningless values in the ratio image. We

simply excluded such pixels with a binary mask derived from the GE images with an intensity threshold which was manually determined. Although we found the resulting ratio images well defined with this procedure, some artifacts are expected to occur on the edges of this mask, due to partial volume between pixels with high PD and pixels with either noise only or very low PD (e.g. inner bone). Imperfect head motion correction for images acquired separately may also yield additional edge artifacts. The potential impact of such edge effects on tissue classification algorithms may have to be investigated, although we rather found that standard segmentation algorithms were working successfully on unbiased P/NP ratio images obtained with the simple mask described above (Olman et al., 2007).

Impact of Receive Coil Arrays

For simplicity we have assumed in the formalism utilized in this paper that signal intensity for both MPRAGE and GE-PD images is proportional to a receive coil sensitivity profile $|\mathbf{B}_1^-|$. When utilizing receive coil arrays, output magnitude images are usually obtained as the root sum of squares (RSOS) of the individual receive coil images for SNR optimization (Roemer et al., 1990). As a result, $|\mathbf{B}_1^-|$ should be replaced with the root sum of squares of the receive coil sensitivities in Eq. [1] and [2]. However, coil sensitivity profiles concern equally the numerator and the denominator, so that P/NP ratio can be directly formed with RSOS images without modification.

Other limitations

3D-MPRAGE sequences inherently induce a distorted point spread function (PSF) in T_1w images due to the evolution of M_{MPRAGE} during the fast train of readout (Deichmann et al., 2000). In the ratio technique proposed here, the 3D-GE image used for the division is acquired in the steady state, thus with very little T_1 related PSF distortion. Forming ratio images does not address MPRAGE related PSF. However, to a large extent, any optimized MPRAGE sequence (Deichmann et al., 2000; Foo et al., 1994) could benefit from the present ratio technique. It should be noted that at higher field, due to longer T_1's, longer TA's can be used with unchanged TA/T_1 ratio. This suggests that higher spatial resolution may be obtained at higher field with MPRAGE sequences without further degrading the T_1 PSF. In this study we did not address the issue of Rician noise distribution in magnitude images. However, in most data presented here, SNR was high enough to make such impact negligible.

Conclusion

We have demonstrated at 7 Tesla that forming the ratio of T_1w images obtained with adiabatic inversion to GE images obtained without preparation is a simple and very efficient way to correct T_1w images for signal variations induced by B_1 profiles, Proton Density and T_2* contrast. Although T_1w MPRAGE images can be corrected for receive B1 profiles with low spatial resolution GE images and appropriate post-processing algorithms, both data need being acquired at high spatial resolution in order to address T_2* and Proton Density induced image alterations, rich in high spatial frequencies. The implementation of the introduced technique is straightforward, it does not require sophisticated post processing algorithms, and corrected T_1w images are produced *in addition to*, but *not instead of*, standard magnetization prepared T_1w images which represent a gold standard reference in brain imaging. Furthermore, we demonstrate that ratio images also have the potential of producing Maximum Intensity Projection angiograms, derived from the same data, thus inherently registered with T_1w structural images.

In order to address *inter-scan* head motion induced artifacts when dividing the two images, a new sequence was developed with the two 3D acquisitions interleaved. Users can choose

between this interleaved approach, which is however more sensitive to *intra-scan* head motion because of a longer single scan acquisition, and the two shorter separate acquisitions, more sensitive to *inter-scan* motion.

It is expected that this simple technique could greatly contribute to the fast growing interest in brain tissue contrast at high field, providing increased T_1 specificity and allowing for comparing data obtained in different sessions, with different RF coils or with different scanners.

Acknowledgments

We are grateful to the anonymous reviewers for their very useful comments and for bringing to our knowledge the work referenced in (van Gelderen et al., 2006). We want to express our acknowledgements to Gregor Adriany for RF coil support. This study was supported by BTRR - P41 RR008079, MIND Institute, NIH-P30 NS05709. R01 MH070800, R01 EB000331

Appendix

Appendix 1:

With the following contrast definition between signals A and B:

$$C_{image}^{A/B}=\frac{A-B}{A+B}=\frac{1-D}{1+D} \quad [16]$$

where $D=\frac{B}{A}$, the WM/GM contrast in either MPRAGE (MP) or in P/NP images becomes:

$$C_{\mathrm{MP,P/NP}}^{W/G}=\frac{1-D_{\mathrm{MP,P/NP}}^{G/W}}{1+D_{\mathrm{MP,P/NP}}^{G/W}}, \quad [17]$$

where

$$D_{\mathrm{MP,P/NP}}^{G/W}=\frac{S_{\mathrm{MP,P/NP}}^{G}}{S_{\mathrm{MP,P/NP}}^{W}}. \quad [18]$$

From Eq. [3] we can write:

$$D_{\mathrm{P/NP}}^{G/W}=\frac{S_{\mathrm{P/NP}}^{G}}{S_{\mathrm{P/NP}}^{W}}=\frac{S_{\mathrm{MP}}^{G}}{S_{\mathrm{MP}}^{W}}\cdot\frac{S_{\mathrm{GE}}^{W}}{S_{\mathrm{GE}}^{G}}=D_{\mathrm{MP}}^{G/W}\cdot\frac{S_{\mathrm{GE}}^{W}}{S_{\mathrm{GE}}^{G}}, \quad [19]$$

where S_{GE} is the signal in GE-PD images

and

$$\frac{S_{\mathrm{GE}}^{W}}{S_{\mathrm{GE}}^{G}}=\frac{\rho^{W}}{\rho^{G}}\cdot\frac{\tilde{M}_{0}^{*W}}{\tilde{M}_{0}^{*G}}. \quad [20]$$

After Eq. [4] and [5] we see that:

$$\frac{M_0^*}{M_0} = \frac{1 - E_{T_1}^{TR}}{1 - E_{T_1^*}^{TR}} \quad [21]$$

For all 3D acquisitions considered here (short TR, small flip angle) we obtain TR≪T1*<T1, which allows the approximation (Deichmann and Haase, 1992; Deichmann et al., 1999):

$$\frac{M_0^*}{M_0} \approx \frac{T_1^*}{T_1} = \frac{1}{1 - T_1 \frac{\ln(\cos\alpha)}{TR}} \quad [22]$$

$$\frac{S_{\mathrm{GE}}^W}{S_{\mathrm{GE}}^G} \approx \frac{\rho^W}{\rho^G} \cdot \frac{T_1^{*W}}{T_1^W} \cdot \frac{T_1^G}{T_1^{*G}} \quad [23]$$

From Eqs. [23] and [22] we define the parameter λ summarizing the sources of contrast changes between WM and GM induced by forming the image ratio. λ is a function of tissue parameters (ρ, T_1) as well as acquisition parameters (TR, α):

$$\lambda\left(\underbrace{T_1^G, T_1^W, \rho^G, \rho^W}_{\text{Tissue Properties}}, \underbrace{TR, \alpha}_{\text{Acquisition}}\right) = \frac{S_{\mathrm{GE}}^W}{S_{\mathrm{GE}}^G} \approx \frac{\rho^W}{\rho^G} \cdot \frac{1 - T_1^G \frac{\ln[\cos\alpha]}{TR}}{1 - T_1^W \frac{\ln[\cos\alpha]}{TR}} \quad [24]$$

Finally, T_1 contrast in P/NP image can be expressed as:

$$C_{\mathrm{P/NP}}^{W/G} = \frac{1 - \lambda D_{\mathrm{MP}}^{G/W}}{1 + \lambda D_{\mathrm{MP}}^{G/W}} \quad [25]$$

References

Adriany, G.; Ritter, J.; Van de Moortele, PF.; Moeller, S.; Snyder, C.; Voje, B.; Vaughan, JT.; Ugurbil, K. A geometrically adjustable 16 Channel Transceive Transmission Line Array for 7 Tesla. ISMRM 13th Scientific Meeting; Miami. 2005a. p. 673

Adriany G, Van de Moortele PF, Wiesinger F, Moeller S, Strupp JP, Andersen P, Snyder C, Zhang X, Chen W, Pruessmann KP, Boesiger P, Vaughan T, Ugurbil K. Transmit and receive transmission line arrays for 7 Tesla parallel imaging. Magnetic Resonance in Medicine. 2005b; 53:434–445. [PubMed: 15678527]

Augustinack JC, van der Kouwe AJ, Blackwell ML, Salat DH, Wiggins CJ, Frosch MP, Wiggins GC, Potthast A, Wald LL, Fischl BR. Detection of entorhinal layer II using 7Tesla [correction] magnetic resonance imaging. Ann Neurol. 2005; 57:489–494. [PubMed: 15786476]

Belaroussi B, Milles J, Carme S, Zhu YM, Benoit-Cattin H. Intensity non-uniformity correction in MRI: existing methods and their validation. Med Image Anal. 2006; 10:234–246. [PubMed: 16307900]

Bernstein MA, Huston J 3rd, Ward HA. Imaging artifacts at 3.0T. J Magn Reson Imaging. 2006; 24:735–746. [PubMed: 16958057]

Bevington, PR. Data Reduction and Analysis for the Physical Sciences. McGraw-Hill; 1969.

Bottomley PA, Andrew ER. RF magnetic field penetration, phase shift and power dissipation in biological tissue: implications for NMR imaging. Physics in Medicine and Biology. 1978; 23:630–643. [PubMed: 704667]

Collins CM, Smith MB. Signal-to-noise ratio and absorbed power as functions of main magnetic field strength, and definition of “90 degrees” RF pulse for the head in the birdcage coil. Magnetic Resonance in Medicine. 2001; 45:684–691. [PubMed: 11283997]

Collins CM, Yang QX, Wang JH, Zhang X, Liu H, Michaeli S, Zhu XH, Adriany G, Vaughan JT, Anderson P, Merkle H, Ugurbil K, Smith MB, Chen W. Different excitation and reception distributions with a single-loop transmit-receive surface coil near a head-sized spherical phantom at 300 MHz. Magnetic Resonance in Medicine. 2002; 47:1026–1028. [PubMed: 11979585]

Deichmann R, Good CD, Josephs O, Ashburner J, Turner R. Optimization of 3-D MP-RAGE sequences for structural brain imaging. NeuroImage. 2000; 12:112–127. [PubMed: 10875908]

Deichmann R, Good CD, Turner R. RF inhomogeneity compensation in structural brain imaging. Magnetic Resonance in Medicine. 2002; 47:398–402. [PubMed: 11810686]

Deichmann R, Haase A. Quantification of T1 values by SNAPSHOT-FLASH NMR Imaging. Journal of Magnetic Resonance. 1992; 96:608–612.

Deichmann R, Hahn D, Haase A. Fast T1 mapping on a whole-body scanner. Magnetic Resonance in Medicine. 1999; 42:206–209. [PubMed: 10398969]

Deichmann R, Schwarzbauer C, Turner R. Optimisation of the 3D MDEFT sequence for anatomical brain imaging: technical implications at 1.5 and 3 T. NeuroImage. 2004; 21:757–767. [PubMed: 14980579]

Foo TK, Sawyer AM, Faulkner WH, Mills DG. Inversion in the steady state: contrast optimization and reduced imaging time with fast three-dimensional inversion-recovery-prepared GRE pulse sequences. Radiology. 1994; 191:85–90. [PubMed: 8134602]

Ge Y, Zohrabian VM, Grossman RI. Seven-Tesla magnetic resonance imaging: new vision of microvascular abnormalities in multiple sclerosis. Arch Neurol. 2008; 65:812–816. [PubMed: 18541803]

Gelman N, Ewing JR, Gorell JM, Spickler EM, Solomon EG. Interregional variation of longitudinal relaxation rates in human brain at 3.0 T: relation to estimated iron and water contents. Magnetic Resonance in Medicine. 2001; 45:71–79. [PubMed: 11146488]

Glover GH, Hayes CE, Pelc NJ, Edelstein WA, Mueller OM, Hart HR, Hardy CJ, O'Donnel M, Barber WD. Comparison of linear and circular polarization for magnetic resonance imaging. J Magn Reson. 1985; 64:255–270.

Haase A. Snapshot FLASH MRI: Application to T_1, T_2, and Chemical Shift Imaging. Magnetic Resonance in Medicine. 1990; 13:77–89. [PubMed: 2319937]

Jenkinson M, Bannister P, Brady M, Smith S. Improved optimization for the robust and accurate linear registration and motion correction of brain images. NeuroImage. 2002; 17:825–841. [PubMed: 12377157]

Just M, Thelen M. Tissue characterization with T1, T2, and proton density values: results in 160 patients with brain tumors. Radiology. 1988; 169:779–785. [PubMed: 3187000]

Kaptein R, Dukstra K, Tarr CE. A Single-Scan Fourier Transform Method for Measuring Spin-Lattice Relaxation Times. Journal of Magnetic Resonance. 1976; 24:295–300.

Katscher U, Bornert P, Leussler C, van den Brink JS. Transmit SENSE. Magnetic Resonance in Medicine. 2003; 49:144–150. [PubMed: 12509830]

Keltner JR, Carlson JW, Roos MS, Wong STS, Wong TL, Budinger TF. Electromagnetic Fields of Surface Coil *in Vivo* NMR at High Frequencies. Magnetic Resonance in Medicine. 1991; 22:46–480.

Larsson, J. Imaging vision: functional mapping of intermediate visual processes in man. Karolinska Institutet; Stockholm, Sweden: 2001.

Laub G. Displays for MR angiography. Magnetic Resonance in Medicine. 1990; 14:222–229. [PubMed: 2345504]

Li TQ, van Gelderen P, Merkle H, Talagala L, Koretsky AP, Duyn J. Extensive heterogeneity in white matter intensity in high-resolution T2*-weighted MRI of the human brain at 7.0 T. NeuroImage. 2006; 32:1032–1040. [PubMed: 16854600]

Mao W, Smith MB, Collins CM. Exploring the limits of RF shimming for high-field MRI of the human head. Magnetic Resonance in Medicine. 2006; 56:918–922. [PubMed: 16958070]

Mugler JP III, Brookman JR. Three dimensional magnetization-prepared rapid gradient-echo imaging (3D MPRAGE). Magnetic Resonance in Medicine. 1990; 15:152–157. [PubMed: 2374495]

Olman, C.; Van de Moortele, PF.; Ugurbil, K.; Yacoub, E. Neuroscience. San Diego: 2007. Retinotopic mapping with 7 Tesla fMRI: improved resolution and decreased experiment duration; p. 768

Peters AM, Brookes MJ, Hoogenraad FG, Gowland PA, Francis ST, Morris PG, Bowtell R. T2* measurements in human brain at 1.5, 3 and 7 T. Magn Reson Imaging. 2007; 25:748–753. [PubMed: 17459640]

Pfeuffer J, Adriany G, Shmuel A, Yacoub E, Van De Moortele PF, Hu X, Ugurbil K. Perfusion-based high-resolution functional imaging in the human brain at 7 Tesla. Magnetic Resonance in Medicine. 2002; 47:903–911. [PubMed: 11979569]

Roemer PB, Edelstein WA, Hayes CE, Souza SP, Mueller OM. The NMR Phased Array. Magnetic Resonance in Medicine. 1990; 16:192–225. [PubMed: 2266841]

Rooney WD, Johnson G, Li X, Cohen ER, Kim SG, Ugurbil K, Springer CS Jr. Magnetic field and tissue dependencies of human brain longitudinal (1)H(2)O relaxation in vivo. Magnetic Resonance in Medicine. 2007; 57:308–318. [PubMed: 17260370]

Setsompop K, Wald LL, Alagappan V, Gagoski B, Hebrank F, Fontius U, Schmitt F, Adalsteinsson E. Parallel RF transmission with eight channels at 3 Tesla. Magnetic Resonance in Medicine. 2006; 56:1163–1171. [PubMed: 17036289]

Smith SM, Jenkinson M, Woolrich MW, Beckmann CF, Behrens TE, Johansen-Berg H, Bannister PR, De Luca M, Drobnjak I, Flitney DE, Niazy RK, Saunders J, Vickers J, Zhang Y, De Stefano N, Brady JM, Matthews PM. Advances in functional and structural MR image analysis and implementation as FSL. NeuroImage. 2004; 23(1):S208–219. [PubMed: 15501092]

Thomas BP, Welch EB, Niederhauser BD, Whetsell WO Jr, Anderson AW, Gore JC, Avison MJ, Creasy JL. High-resolution 7T MRI of the human hippocampus in vivo. J Magn Reson Imaging. 2008; 28:1266–1272. [PubMed: 18972336]

Van de Moortele, PF.; Auerbach, EJ.; Olman, C.; Yacoub, E.; Ugurbil, K.; Moeller, S. Which clinical application(s) would best benefit from submillimeter High T1 contrast whole brain images at 7Tesla with simultaneous angiography perfectly coregistered with anatomical images?. Unsolved Problems and Unmet Needs Symposium; ISMRM 14th Annual meeting; Toronto. 2008a. p. 172

Van de Moortele PF, Akgun C, Adriany G, Moeller S, Ritter J, Collins CM, Smith MB, Vaughan JT, Ugurbil K. B(1) destructive interferences and spatial phase patterns at 7 T with a head transceiver array coil. Magnetic Resonance in Medicine. 2005; 54:1503–1518. [PubMed: 16270333]

Van de Moortele, PF.; Auerbach, EJ.; Olman, C.; Yacoubd, E.; Ugurbil, K.; Moeller, S. Unbiased High Resolution T1 Weighted Brain Images at High Field with a New Interleaved 3D-MPRAGE/ Proton Density GE sequence. Human Brain Mapping 14th Annual Meeting; Sidney. 2008b.

Van de Moortele, PF.; Moeller, S.; Ugurbil, K. Efficient Bias Reduction for High Resolution T1w Imaging in the Human Brain at 7 Tesla. ISMRM Workshop on Advances in High Field MR; Asilomar. 2007.

van Gelderen, P.; Koretsy, AP.; de Zwart, JA.; Duyn, JH. A Simple B_1 Correction Method for High Resolution Neuroimaging. 14th Scientific Meeting ISMRM; Seattle, WA. 2006. p. 2355

Vaughan JT, Adriany G, Snyder CJ, Tian J, Thiel T, Bolinger L, Liu H, DelaBarre L, Ugurbil K. Efficient high-frequency body coil for high-field MRI. Magnetic Resonance in Medicine. 2004; 52:851–859. [PubMed: 15389967]

Vaughan JT, Garwood M, Collins CM, Liu W, DelaBarre L, Adriany G, Andersen P, Merkle H, Goebel R, Smith MB, Ugurbil K. 7T vs. 4T: RF power, homogeneity, and signal-to-noise comparison in head images. Magnetic Resonance in Medicine. 2001; 46:24–30. [PubMed: 11443707]

Wang J, Qiu M, Constable RT. In vivo method for correcting transmit/receive nonuniformities with phased array coils. Magnetic Resonance in Medicine. 2005; 53:666–674. [PubMed: 15723397]

Warntjes JBM, Dahlqvist O, Lundberg P. Novel Method for Rapid, Simultaneous T1, T*2, and Proton Density Quantification. Magnetic Resonance in Medicine. 2007; 57:528–537. [PubMed: 17326183]

Wiesinger F, Van de Moortele PF, Adriany G, De Zanche N, Ugurbil K, Pruessmann KP. Parallel imaging performance as a function of field strength--an experimental investigation using electrodynamic scaling. Magnetic Resonance in Medicine. 2004; 52:953–964. [PubMed: 15508167]

Yacoub E, Shmuel A, Pfeuffer J, Van De Moortele PF, Adriany G, Andersen P, Vaughan JT, Merkle H, Ugurbil K, Hu X. Imaging brain function in humans at 7 Tesla. Magnetic Resonance in Medicine. 2001; 45:588–594. [PubMed: 11283986]

Yarnykh VL. Actual flip-angle imaging in the pulsed steady state: a method for rapid three-dimensional mapping of the transmitted radiofrequency field. Magnetic Resonance in Medicine. 2007; 57:192–200. [PubMed: 17191242]

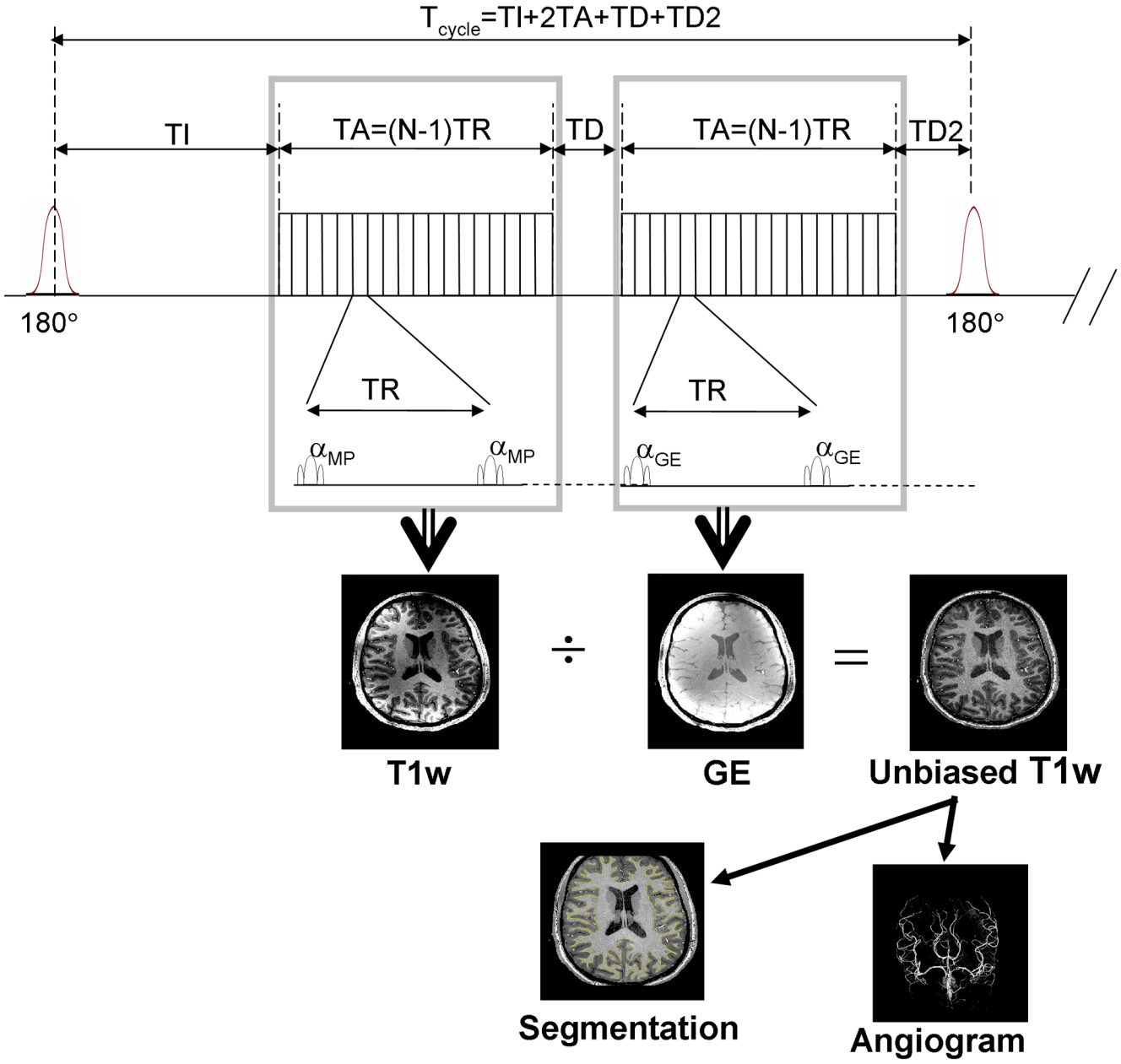

Fig. 1. Interleaved 3D-MPRAGE and 3D-GE Sequence diagram

The first part of the sequence is a standard 3D MPRAGE, with a train of N small flip angle RF pulses (α) following each adiabatic inversion RF pulse (180°). *TI*=inversion time, *TA*=duration of the fast gradient echo train, *TR*=repetition time during the fast gradient echo trains, *TD*=optional delay. The interleaved version includes the second part which consists in repeating the fast gradient echo train (with all parameters identical expect for optional variations between α_{MP} and α_{GE}) followed by an optional delay *TD2* immediately preceding the next inversion pulse (*TD2* typically is zeroed). This cycle is repeated along the loop of the 3rd k-space dimension. α_{MP} and α_{GE} are the small flip angle during the fast echo train of MPRAGE and GE.

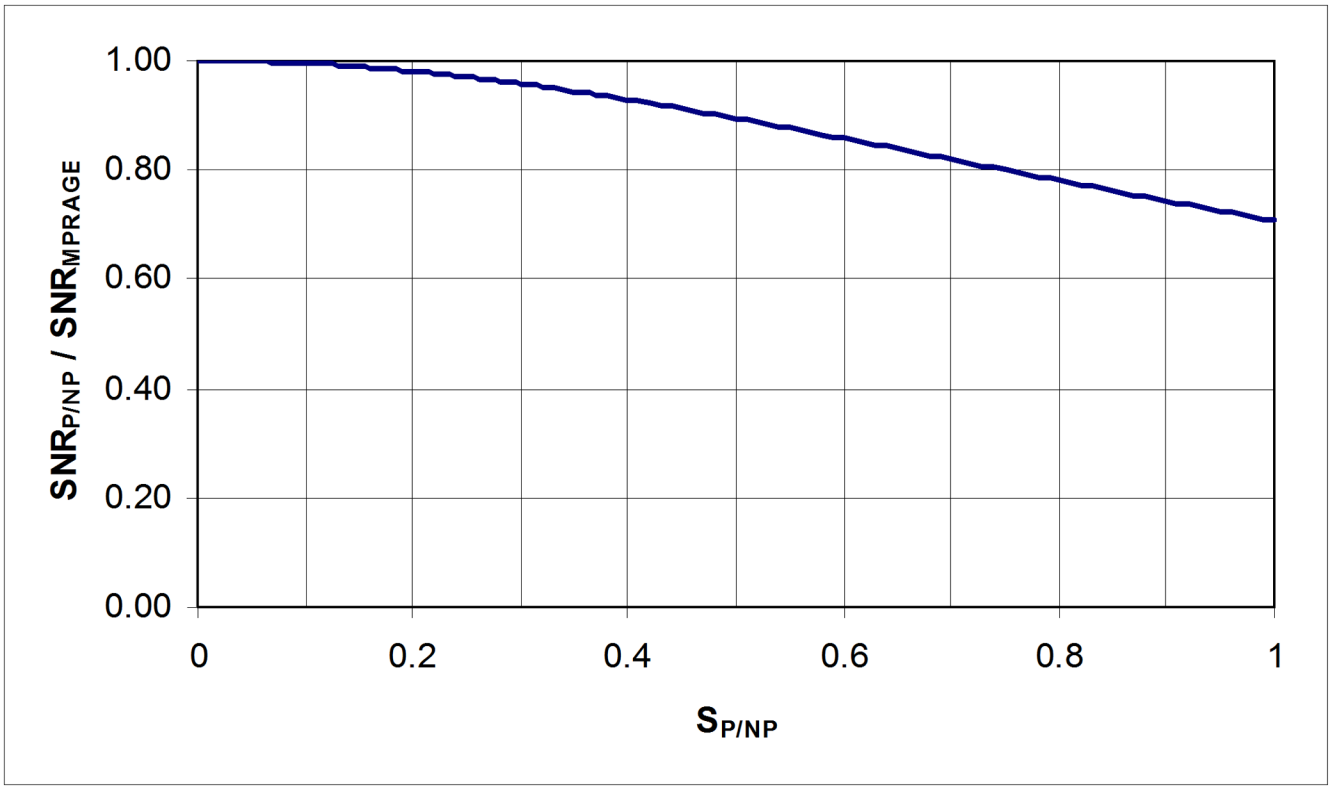

Fig. 2. SNR in P/NP maps as a function of SNR in MPRAGE images

Ratio of Signal to Noise Ratio (SNR) in P/NP maps ($SNR_{P/NP}$) over SNR in MPRAGE images (SNR_{MPRAGE}) as a function of Signal Intensity in P/NP maps ($S_{P/NP}$). Typical values for $S_{P/NP}$ are about 0.65 for white matter and 0.35 for gray matter, with corresponding relative loss in SNR of ~16% and ~6% respectively.

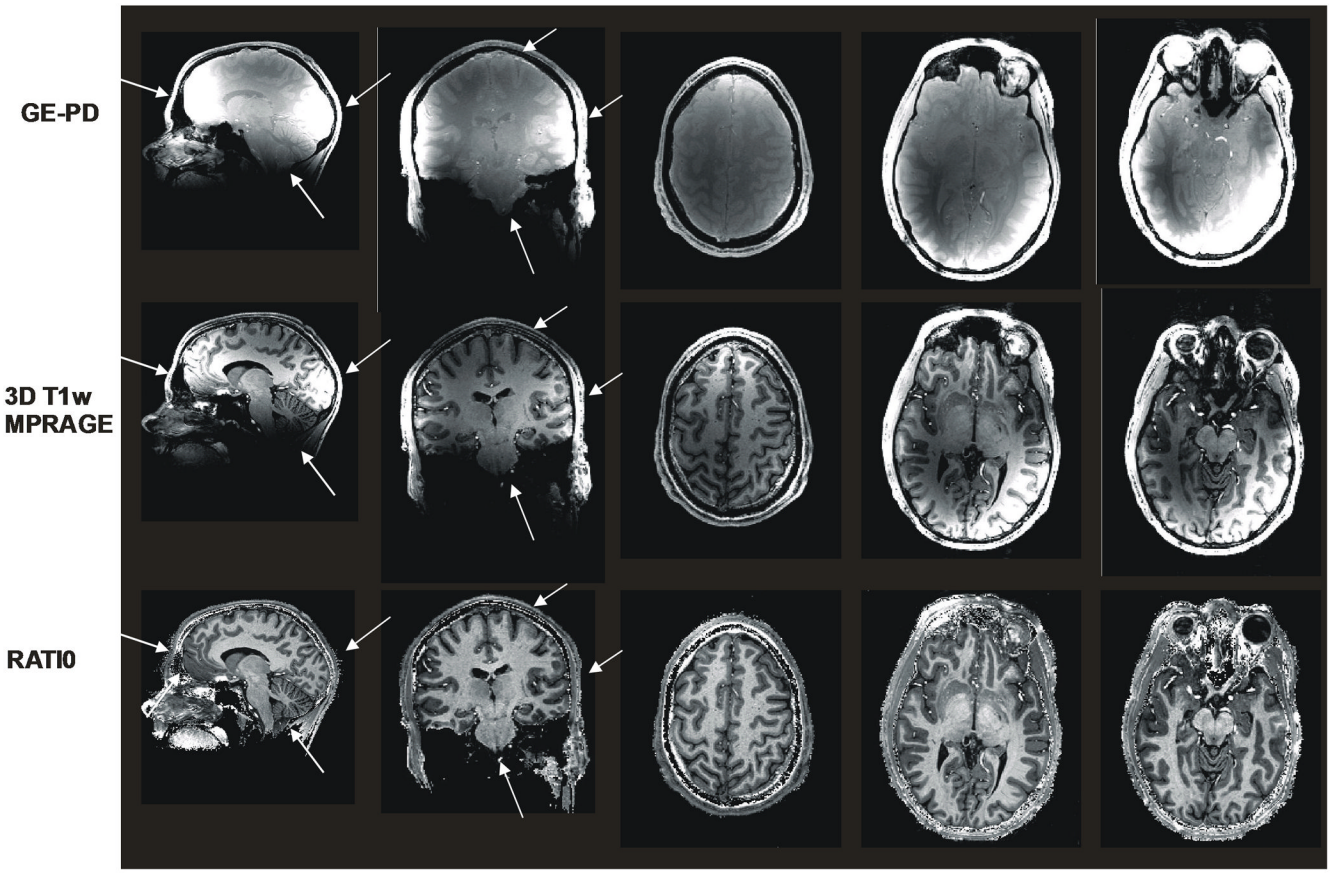

Fig. 3. Whole Brain T1w Imaging at 7 Tesla (α = 3°)

Sagittal, coronal and axial views from a 3D Isotropic (1×1×1mm3) data set at 7Tesla. ***Top row***: 3D GE-PD ***Middle row***:3D MPRAGE ***Bottom row***: P/NP ratio. White arrows indicate areas brighter or darker in MPRAGE and GE images which do not exhibit such regional intensity variation in ratio images. For some of those areas, such as cerebellum or anterior frontal lobe, identifying gray/white matter contrast without correction can be difficult. MPRAGE and GE-PD images were acquired separately with following acquisition parameters: TI_{Siemens}=1.5ss (MPRAGE only), *TD*=1.3s (MPRAGE only), *TA*= 1.34s, nominal flip angle: 3°. Scan times: 10min45s (MPRAGE) and 5min45s (GE). Note that GE-PD images are clearly dominated with Proton Density contrast (gray matter brighter than white matter). No motion correction was needed with this particular data set.

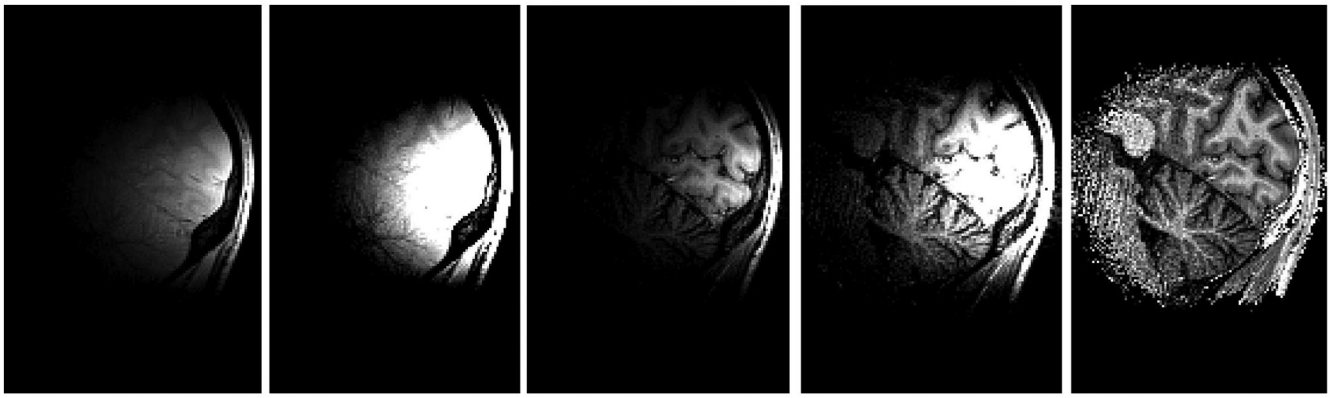

Fig. 4. Surface Coil data at 7 Tesla

Sagittal view of GE-PD (two leftmost images), MPRAGE (next two images to the right) and P/NP map (single rightmost image) obtained from a 3D isotropic data set (1×1×1mm3 spatial resolution) in the occipital lobe at 7 Tesla. Whereas a single gray scale is sufficient to show the whole range of signal in the rightmost P/NP image, it is necessary to display the same image with two different gray scales for both GE-PD and MPRAGE in order to visualize the full range of tissues from darkest to brightest areas. Note the tremendous improvement in gray/white matter visibility in the rightmost P/NP map with high T_1 contrast. The better noise visibility in low SNR areas should not be interpreted as noise amplification (see Methods). Images were acquired separately with standard MPRAGE and GE sequence: TI_{Siemens}=1.5s (MPRAGE only), TD=0.94s (MPRAGE only), TA= 1.12s, nominal flip angle: 3°. Scan time: 6min26s (MPRAGE) and 2min25s (GE).

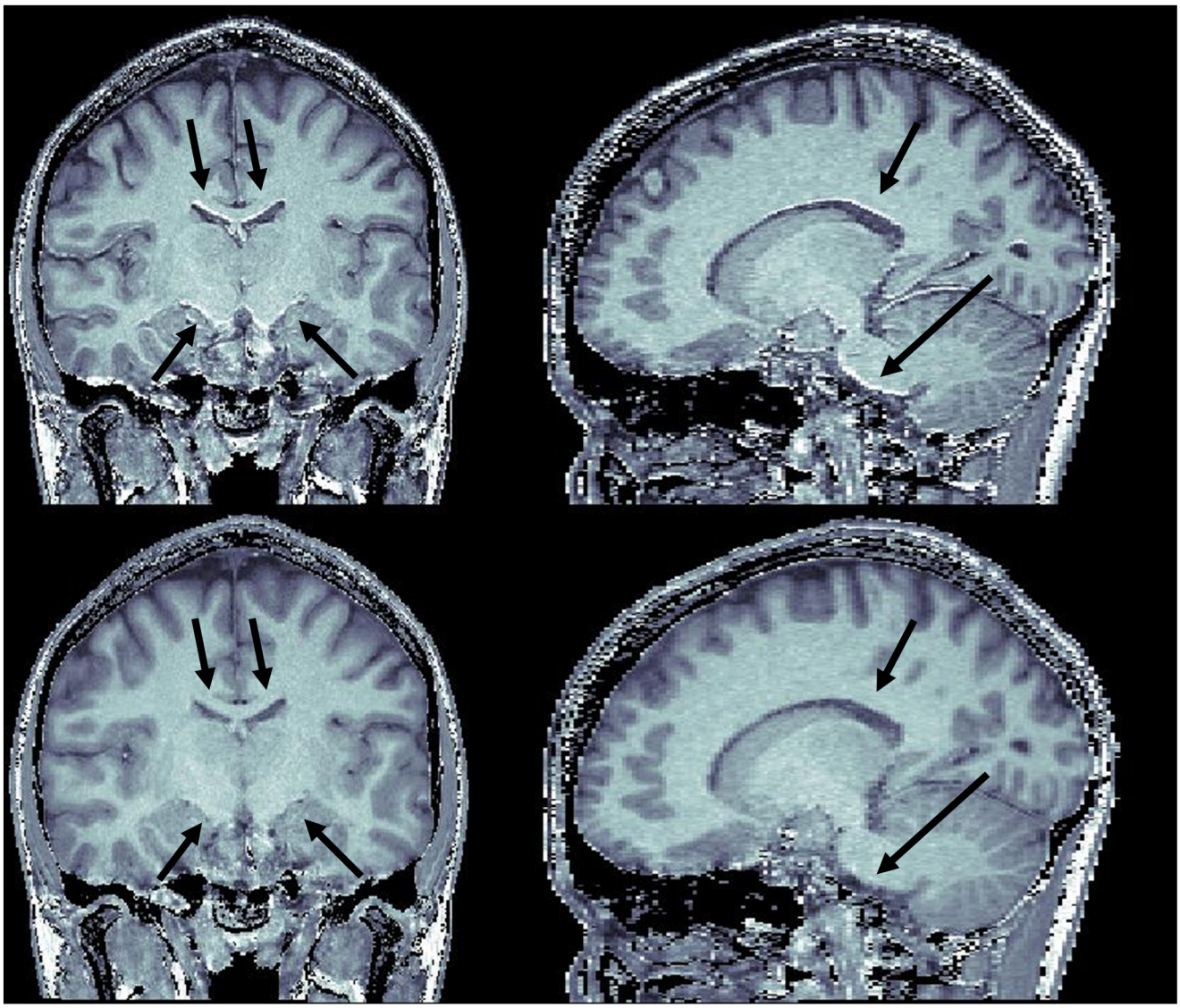

Fig. 5. Head Motion

P/NP ratio images without and with head motion correction. Corresponding MPRAGE and GE images were acquired with $0.65\times0.65\times1.5mm^3$ voxel size. Scan time was 10min49s for MPRAGE and 8min8s for GE. MPRAGE image was realigned onto GE image with the FLIRT package (see Methods). ***Top row***: coronal and parasagittal views of P/NP ratio formed with uncorrected MPRAGE and GE images. Note the numerous edge artifacts (brighter edges are easier to identify than darker edges), some of them signaled with arrows. ***Bottom row***: coronal and parasagittal views of the ratio between realigned MPRAGE and GE. The edge artifacts are not visible anymore (see arrows).

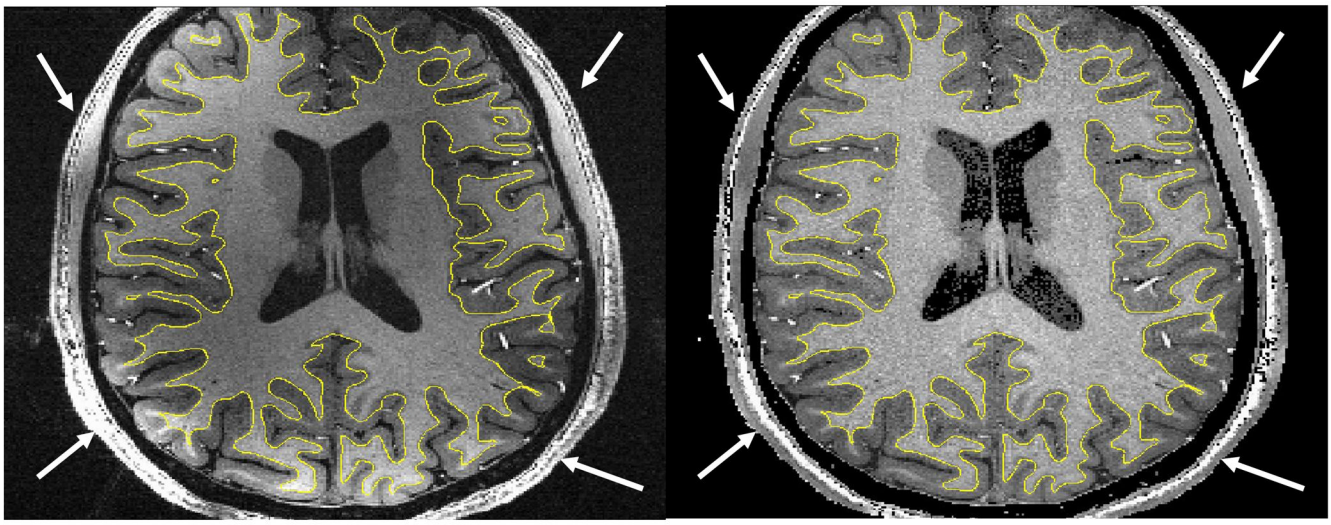

Fig. 6. Brain segmentation with high resolution data

Axial view of 3D-MPRAGE (left) and of corresponding P/NP ratio (right) images from isotropic 3D data sets ($0.65\times0.65\times0.65=0.27\text{mm}^3$ spatial resolution) obtained at 7T. 3D-MPRAGE (left) and 3D-GE (not shown) images were simultaneously acquired with the double contrast interleaved sequence with GRAPPA R=2 along the Y axis (TI_{Siemens}=1.5s, T_{cycle}=4.1s, TR=11.4ms, total scan time 14min12s). With non corrected 3D-MPRAGE volume (left) the SurfRelax package failed, even after spatial smoothing, to perform whole brain segmentation because of large signal inhomogeneities. The same procedure applied on P/NP ratio (right) resulted, even without spatial smoothing, in reliable gray/white matter segmentation (yellow contour overlaid on both images). Both images are deliberately shown without spatial filtering. Signal variations in the skin are also largely reduced in P/NP ratio (right) (see arrows), facilitating skin and skull striping procedures. The field of view is truncated along Y axis because of matrix size limits in our current implementation of the segmentation software.

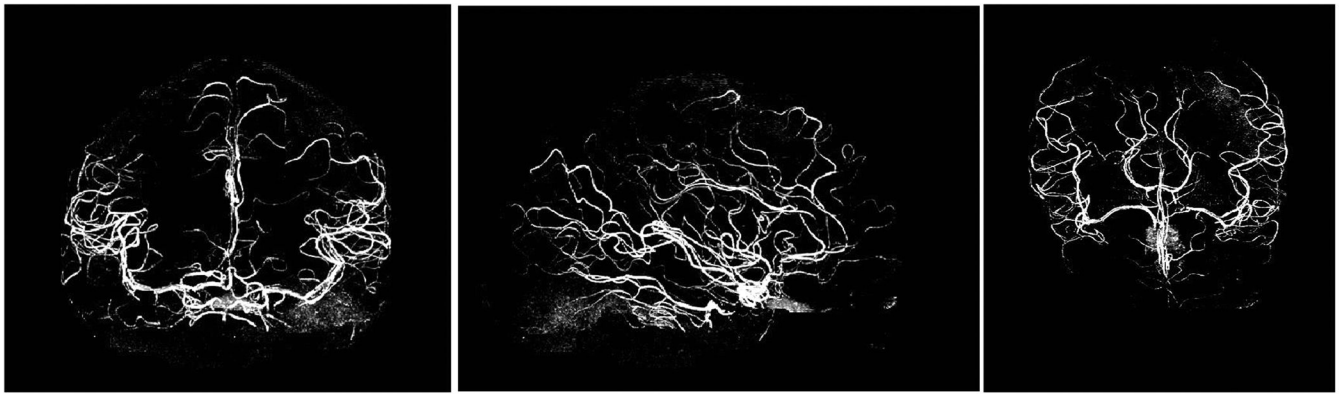

Fig. 7. Maximum Intensity Projection angiogram

Coronal, sagittal and axial projection (from left to right) of Maximum Projection Intensity angiogram obtained at 7 Tesla from P/NP ratio images. Corresponding 3D MPRAGE and 3D GE isotropic data sets ($0.65\times0.65\times0.65=0.27\text{mm}^3$ spatial resolution) were obtained with the interleaved double contrast sequence, with GRAPPA R=2 along Y axis (TI_{Siemens}=1.5s, T_{cycle}=4.1s, TR=11.4ms, total scan time 14min12s). Before forming the ratio, both MPRAGE and GE images were zerofilled, and then GE images were smoothed with a 3D Gaussian kernel (~1.5mm FWHM). Skin and skull as well as other non cerebral structures were removed with 3D morphomathematical tools and an intensity threshold was used to retain vessels pixels.

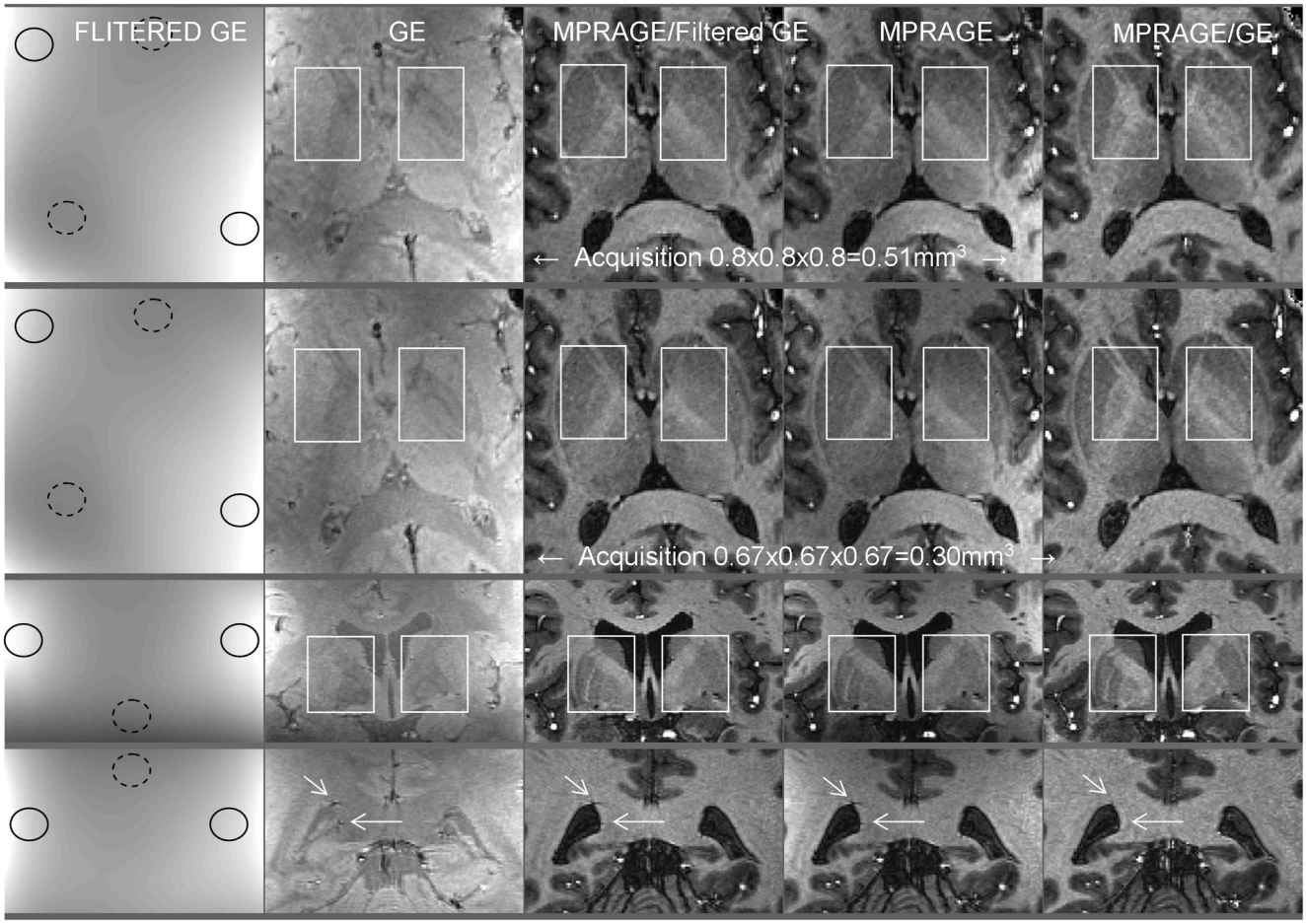

Fig. 8. Low resolution versus matching high resolution reference image (I)

Axial (upper two rows) and coronal (lower two rows) views from high resolution 3D MPRAGE (fourth column) and 3D GE (second column) images acquired with the interleaved sequence. The first column shows GE images convolved with a 27.5×27.5mm2 FWHM Gaussian filter. Plain (dashed) circles signal areas of higher (lower) signal intensity due to receive B1 profile. Ratio images shown in third (fifth) column were obtained by dividing MPRAGE with the filtered (unfiltered) GE images. White boxes and arrows: see text in Result section. **Acquisition parameters**. *Upper row*: voxel size 0.8 × 0.8 × 0.8 = 0.51mm^3, GRAPPA R=3, Partial Fourier [X,Y] = [6/8,6/8], $TI_{Siemens}$=1.5s, T_{cycle}=5.644s, TR=9.8ms, TE=4.45ms, bandwidth=140Hz/pixel, total scan time=7min12s. *Second to fourth row*: voxel size 0.67 × 0.67 × 0.67 = 0.30mm^3, GRAPPA R=3, Partial Fourier [X,Y] = [6/8,6/8], $TI_{Siemens}$=1.5s, T_{cycle}=5.843s, TR=9.8ms, TE=4.45ms, bandwidth=140Hz/pixel, total scan time=11min24s.

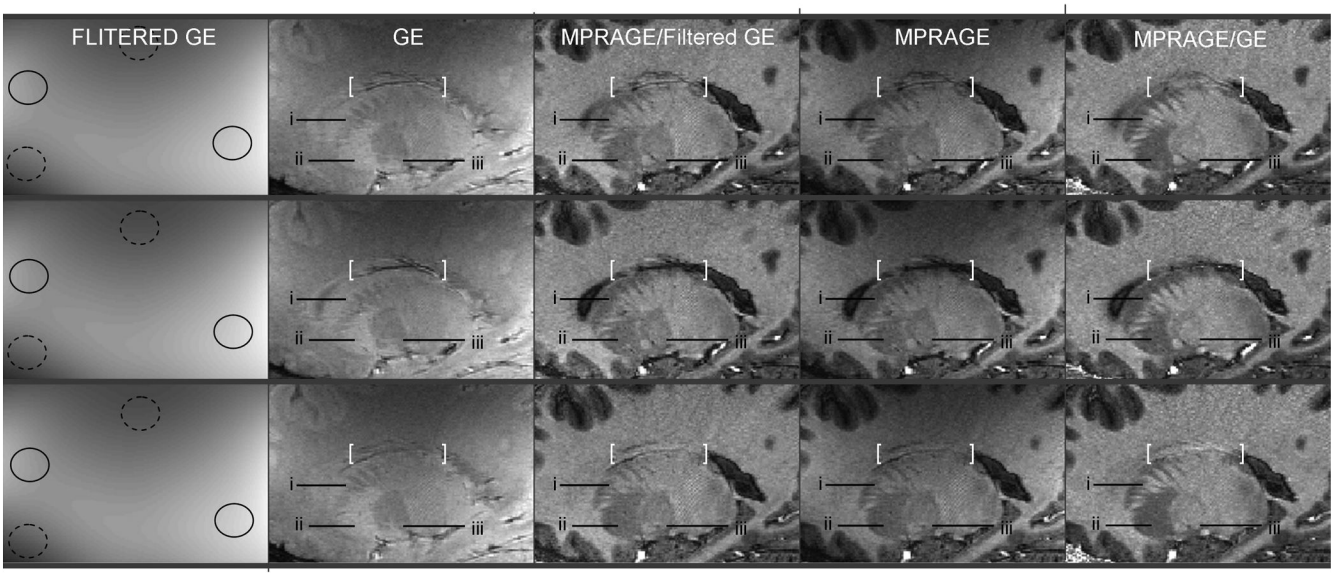

Fig. 9. Low resolution versus matching high resolution reference image (II)

Three contiguous parasagittal views (one per row) from high resolution 3D MPRAGE (fourth column) and 3D GE (second column) images acquired with the interleaved sequence. The first column shows GE images convolved with a 27.5×27.5mm2 FWHM Gaussian filter. Plain (dashed) circles signal areas of higher (lower) signal intensity due to receive B1 profile. Ratio images shown in third (fifth) column were obtained by dividing MPRAGE with the filtered (unfiltered) GE images. White brackets and labels: see text in Result section. **Acquisition parameters**: voxel size 0.67 × 0.67 × 0.67 = 0.30mm^3, GRAPPA R=2, Partial Fourier [X,Y] = [6/8,6/8], TI_{Siemens}=1.5s, T_{cycle}=6.870s, TR=15ms, TE=5.74ms, bandwidth=140Hz/pixel, total scan time=13min24s. Note that this data set was collected with the "whisper" gradient option of the console for reducing acoustic noise, resulting in a longer TR (15ms).

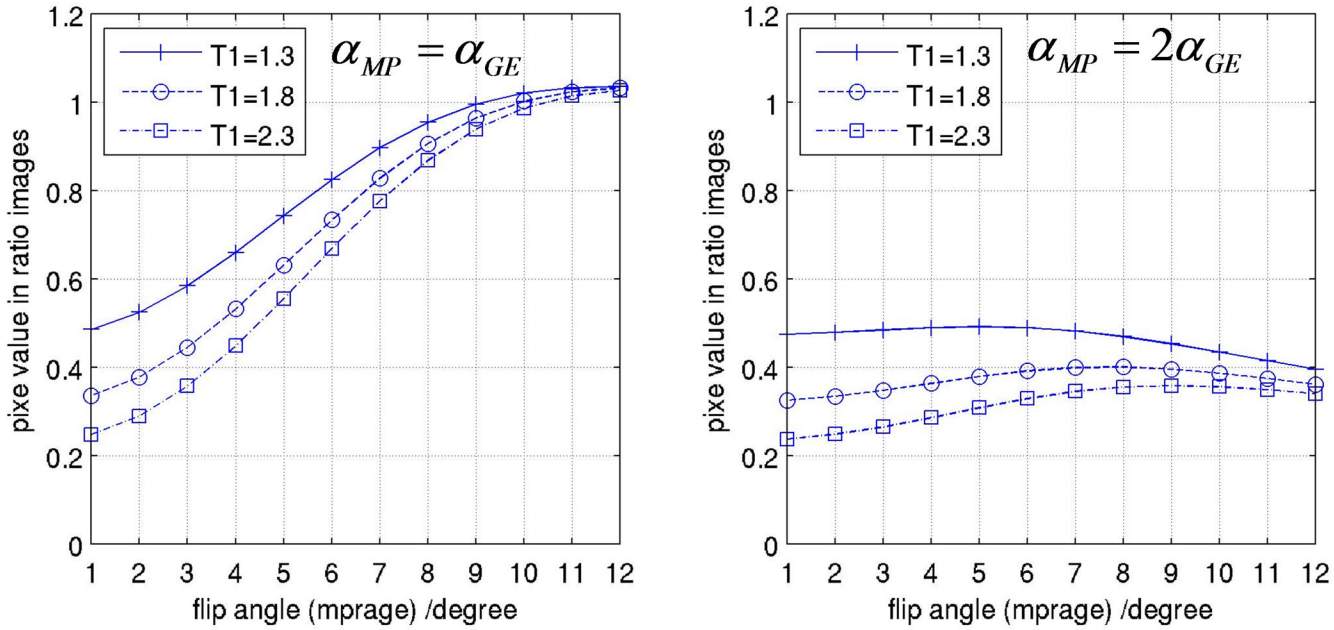

Fig. 10. Simulation: prediction of P/NP value as a function of α

Predicted value of P/NP (at k-space center) based on simulations for three different T_1: 1.3s (crosses), 1.8s (circles) and 2.3s (squares). *Left*: predicted values in P/NP maps when MPRAGE and GE are acquired with same value for α. *Right*: predicted values in P/NP maps when MPRAGE is acquired with α set to the value shown in the abscissa, whereas GE is acquired with the flip angle set to one half of this value. All other parameters were taken from the data shown in Fig. 3: *TI*=0.9s, *TA*=1.35s, *TR*=6ms, *TD*=0.4s, isotropic resolution (1×1×1mm3).

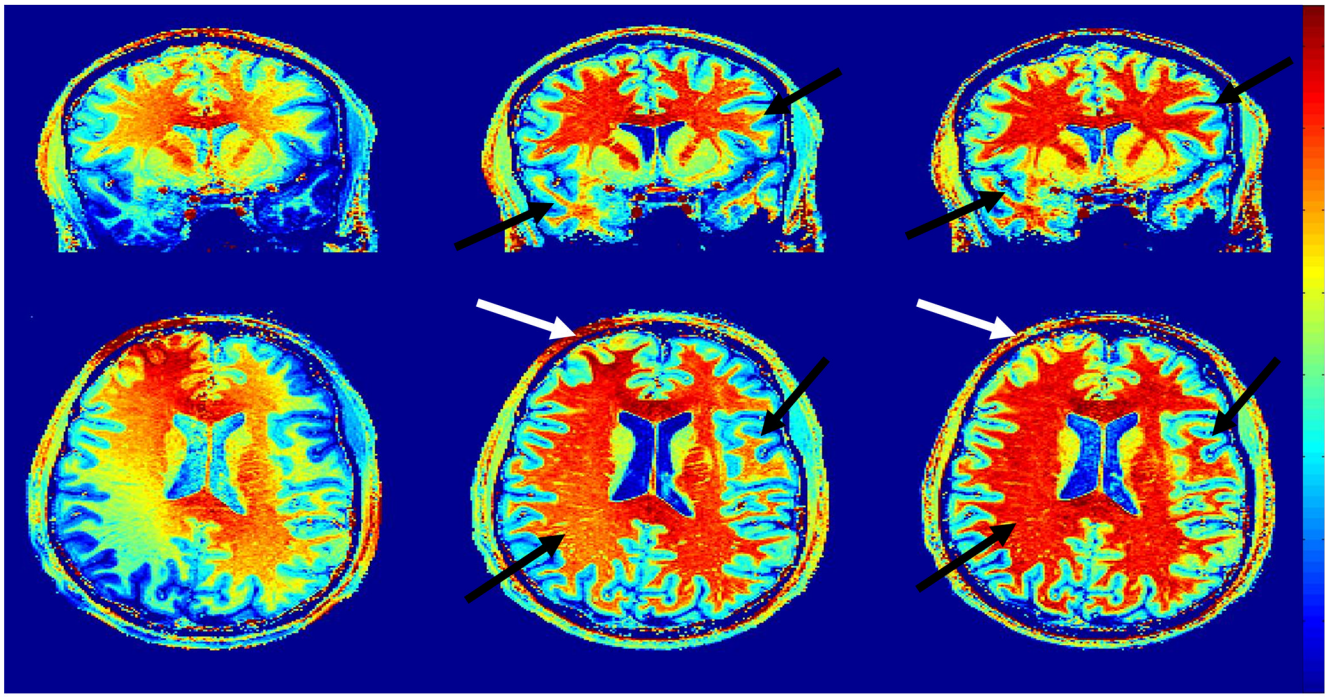

Fig. 11. Residual Transmit B1 induced bias

Coronal (top) and axial (bottom) views of different P/NP ratio images derived from data sets acquired with different small flip angle (α) values at 7 Tesla, demonstrating the impact of the latter onto residual Transmit B1 induced bias. ***Left***: MPRAGE[α=6°]/GE[α=6°], ***Middle***: MPRAGE[α=3°]/GE[α=3°], ***Right***: MPRAGE[α=6°]/GE[α=3°]. A too large nominal flip angle (*left*: 6/6) translates into residual intensity bias whose spatial pattern is consistent with magnitude transmit B1 profile obtained with similar RF coils at 7T (see text). Simply using a smaller nominal a (*middle*: 3°/3°) reduces considerably the amplitude of transmit B1 induced residual bias. Utilizing a larger a in MPRAGE than in GE (*right*: 6°/3°) attenuates even further this residual artifact both in location with residual brighter (white arrows) or darker (black arrows) signal intensity. All data were obtained with the same volunteer during one imaging session, with standard MPRAGE or GE sequence at isotropic spatial resolution (1×1×1mm3). Acquisition time was 10min45s for 3D-MPRAGE and 5min45s for 3D-GE. Color scales, in arbitrary units, were adjusted for each data set in order to reach dark red levels within corpus callosum in axial views.

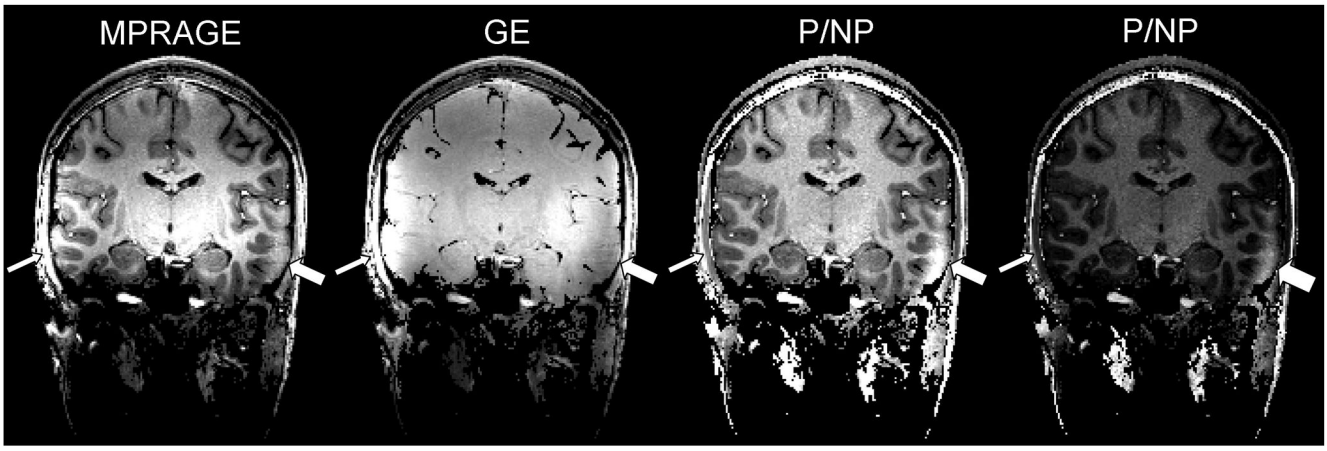

Fig. 12. Identifying adiabatic inversion failure

Coronal view from 3D isotropic (1×1×1mm3) images at 7 Tesla. 3D-MPRAGE and 3D-GE images were simultaneously acquired with the interleaved sequence (GRAPPA acceleration X3, nominal flip angle 4°, total acquisition time 4min54s). From left to right: MPRAGE, GE, NP/P ratio (gray scale 1), NP/P ratio (gray scale 2). An area of low T1 contrast in MPRAGE, signaled with the large arrow, results from local weak $|B_1+|$ below adiabatic threshold. This is significantly easier to identify in P/NP ratio where this area appears clearly brighter than white and gray matter tissue in other locations. Looking at the GE images helps confirming a lower SNR in the same area. The same P/NP ratio image is displayed with two different gray scales in order to better visualize, on the rightmost image, the clear gap in signal intensity between the spot of failed adiabatic inversion and the rest of brain tissues. By contrast, signal intensity of this area in MPRAGE is close to that of white matter in other parts of the brain.

Table 1
Contrast components in MPRAGE, PD-GE and P/NP ratio

The main signal components in the 3 different images considered in this study (with [P/NP]=[MPRAGE]/[PD-GE]) can be split into three categories:
A: Uniform and strong T_1-weighted contrast (T_1w) induced by the adiabatic inversion pulse, completely absent from PD-GE, unaltered in the Ratio. **B**: Components varying through space but identical in MPRAGE and GE-PD, thus vanishing in P/NP maps: PD (Proton Density), T_2*, $|\mathbf{B}_1^-|$ (receive B_1 sensitivity profile), sin(α) with $\alpha \propto |\mathbf{B}_1^+|$ (transmit B_1 sensitivity profile). **C**: T_1-weighted components due to a which varies through space with more complicated expression differing in MPRAGE (§) and GE-PD (†), thus with an impact on P/NP (‡) which varies through space and with acquisition parameters. Signal variation due to this component, however, is typically of limited amplitude compared with components listed in category B.

		PD-GE	MP-RAGE	P/NP
A	IR-T_1w	-	+	+
B	PD	+	+	-
	T_2*	+	+	-
	$\|B_1^-\|$	+	+	-
	Sin(α)	+	+	-
C	Fast GE T_1w	+§	+†	+‡